

INVERSION OF THE ATTENUATED MOMENTA RAY TRANSFORM OF PLANAR SYMMETRIC TENSORS

HIROSHI FUJIWARA, DAVID OMOGBHE, KAMRAN SADIQ, AND ALEXANDRU TAMASAN

ABSTRACT. We present a reconstruction method that stably recovers the real valued, symmetric tensors compactly supported in the Euclidean plane, from knowledge of their attenuated momenta ray transform. The problem is recast as an inverse boundary value problem for a system of transport equations, which we solve by an extension of Bukhgeim's A -analytic theory. The method of proof is constructive. To illustrate the reconstruction method, we present results obtained in the numerical implementation for the non-attenuated case of 1-tensors. This new version now includes the results of the preprint arXiv: 2307.10758.

1. INTRODUCTION

We consider the problem of recovering a real valued, symmetric m -tensor field \mathbf{f} compactly supported in the plane, $m \geq 1$, from knowledge of its $0, 1, \dots, m$ -th attenuated moment ray transforms. This problem is motivated by some engineering applications: for $m = 1$ in Doppler tomography [28, 7, 39], and Magneto-acousto-electrical tomography [17, 23], for $m = 2$ in inverse kinematic problems in isotropic elastic media [1, 18] and for $m = 4$ in anisotropic media [2, 37]. The non-attenuated case also arises in the linearization of the boundary rigidity problem [37, 40, 41].

When the data is limited to the 0-moment, the (non-attenuated) ray transform has a large kernel containing all the potential tensors $d\mathbf{g}$ with \mathbf{g} vanishing at the boundary of the support, and a vast literature in tensor tomography concerns the recovery of the solenoidal part of the field, see [37, 30, 29, 36, 19] and references therein.

In order to recover the entire tensor, three types of additional data have been proposed: some longitudinal ray data as in [37], some transverse data as in [13, 24, 23], or a mixture of the two types [9]. This work concerns the longitudinal data case: In [37] it is shown that the entire field is uniquely determined from the combined k^{th} -moment ray transform for $0 \leq k \leq m$; for brevity we call it the momenta ray transform. Inversion of the momenta ray transform has been the subject of recent research interests: in the Euclidean setting some inversion formulas were given in [10, 11], with reconstruction for the $m = 1$ case in [4, 23], and the recent sharp stability estimates in [12]. In the non-Euclidean setting the unique determination result was shown for simple real analytic Riemannian manifolds in [3], extended to simple Riemannian surface in [22], with inversion for $m = 1$ and sources on a curve in [25], and stability estimates in [38, 21]. Since we also consider the attenuated case, it should be mentioned that the 0-moment attenuated Doppler transform in the Euclidean plane is known to uniquely determine the entire field in subdomains where the attenuation is positive [6, 20, 42]; note, however, that those methods become unstable for small attenuation.

Different from the above referenced works, herein we give a reconstruction method that recovers the entire \mathbf{f} without appealing to the Helmholtz decomposition; in bounded domains this is an advantage

Date: May 9, 2024.

2020 Mathematics Subject Classification. Primary: 44A12, 35J56; Secondary: 45E05.

Key words and phrases. X -ray transform, ray transform of symmetric tensors, k -momentum ray transform, momenta ray transform, A -analytic maps.

that avoids the ambiguity of a harmonic potential. Our approach considers a new inverse source problem for a weakly coupled system of transport equations, which we solve by an extension of Bukhgeim's theory of A -analyticity [8]. Stability estimates for the reconstruction require new higher order a priori estimates for solutions of the Bukhgeim-Beltrami equation. Of independent interest, these estimates introduce a new analytical tool; see Section 3.

In the end we present the results obtained by applying the reconstruction method to three numerical examples in the $m = 1$ (Doppler) case. The analysis of the numerical algorithms involved is subject to a separate discussion.

2. STATEMENT OF THE MAIN RESULT

In this section we introduce notation and state our main result. Let Ω be the unit disc with boundary Γ . For $m \geq 1$ fixed integer, let $\mathbf{f} = (f_{i_1 i_2 \dots i_m})$ be a real valued symmetric m -tensor supported in $\bar{\Omega}$. Furthermore, for $s \geq 1$, we assume that \mathbf{f} has components in the Sobolev space of functions of square integrable derivatives which, up to order s , vanish at the boundary. We denote the space of such tensors by $H_0^s(\mathbf{S}^m; \Omega) = \{\mathbf{f} = (f_{i_1 \dots i_m}) \in \mathbf{S}^m(\Omega) : f_{i_1 \dots i_m} \in H_0^s(\Omega)\}$. The symmetry refers to $f_{i_1 i_2 \dots i_m}$ being invariant under any transposition of the indexes $i_1, \dots, i_m \in \{1, 2\}$.

With the summation convention understood over repeated indexes, for $(x, \boldsymbol{\theta}) \in \mathbb{R}^2 \times \mathbb{S}^1$ we denote by $\langle \mathbf{f}(x), \boldsymbol{\theta}^m \rangle = f_{i_1 \dots i_m}(x) \theta^{i_1} \cdot \theta^{i_2} \dots \theta^{i_m}$ the action of \mathbf{f} on $\underbrace{\boldsymbol{\theta} \otimes \boldsymbol{\theta} \otimes \dots \otimes \boldsymbol{\theta}}_m$.

As in [12] (defined for $a = 0$), in here we work with the k^{th} -moment attenuated ray transform

$$(2.1) \quad I_a^k \mathbf{f}(x, \boldsymbol{\theta}) := \int_{-\infty}^{\infty} t^k e^{-\int_t^{\infty} a(\Pi_{\boldsymbol{\theta}}(x) + s\boldsymbol{\theta}) ds} \langle \mathbf{f}(\Pi_{\boldsymbol{\theta}}(x) + t\boldsymbol{\theta}), \boldsymbol{\theta}^m \rangle dt, \quad 0 \leq k \leq m,$$

where $\Pi_{\boldsymbol{\theta}}(x) = x - (x \cdot \boldsymbol{\theta})\boldsymbol{\theta}$ is the projection of x onto $\boldsymbol{\theta}^\perp$. Both the tensor \mathbf{f} and the function a in (2.1) are assumed extended by zero outside Ω . The function a in (2.1) models an attenuation. In the non-attenuated case ($a = 0$), we use the notation $I^k \mathbf{f} := I_0^k \mathbf{f}$. Note that in the non-attenuated case the definition (2.1) is slightly different than the original definition in [37]: therein for $k \geq 1$ the k^{th} moment ray transform is not constant along the lines (the derivative at x in the direction of $\boldsymbol{\theta}$ does not vanish).

The following elementary result (see the Appendix A for a proof) reduces the inversion of the momenta ray transform to an inverse boundary value problem for a system of transport equations. Let $\Gamma_\pm := \{(x, \boldsymbol{\theta}) \in \partial\Omega \times \mathbb{S}^1 : \pm \nu(x) \cdot \boldsymbol{\theta} > 0\}$ be the incoming (-), respectively outgoing (+), unit tangent sub-bundles of the boundary; where $\nu(x)$ is the outer unit normal at $x \in \partial\Omega$.

Proposition 2.1. *Let $s \geq 0$ and $m \geq 1$ be arbitrarily fixed, and let $\mathbf{f} \in H_0^s(\mathbf{S}^m; \Omega)$ and $a \in C^{s, \mu}(\bar{\Omega})$, $\mu > 1/2$. The system*

$$(2.2a) \quad \boldsymbol{\theta} \cdot \nabla u^0(z, \boldsymbol{\theta}) + a(z)u^0(z, \boldsymbol{\theta}) = \langle \mathbf{f}(z), \boldsymbol{\theta}^m \rangle, \quad \text{for } (z, \boldsymbol{\theta}) \in \bar{\Omega} \times \mathbb{S}^1,$$

$$(2.2b) \quad \boldsymbol{\theta} \cdot \nabla u^k(z, \boldsymbol{\theta}) + a(z)u^k(z, \boldsymbol{\theta}) = u^{k-1}(z, \boldsymbol{\theta}), \quad \text{for } 1 \leq k \leq m,$$

subject to

$$(2.2c) \quad u^k|_{\Gamma_-} = 0, \quad 0 \leq k \leq m,$$

has a unique solution $u^k \in H^s(\Omega \times \mathbb{S}^1)$. In particular, if $s \geq 1$, then $u^k|_{\Gamma \times \mathbb{S}^1} \in H^s(\mathbb{S}^1; H^{s-\frac{1}{2}}(\Gamma))$.

Moreover, $\langle u^0|_{\Gamma_+}, u^1|_{\Gamma_+}, \dots, u^m|_{\Gamma_+} \rangle$ are in a one-to-one correspondence with the attenuated momenta ray transform $\langle I_a^0 \mathbf{f}, I_a^1 \mathbf{f}, \dots, I_a^m \mathbf{f} \rangle$ in (2.1) via the relations

$$(2.3) \quad \begin{aligned} u^0|_{\Gamma_+}(x, \boldsymbol{\theta}) &= I_a^0 \mathbf{f}(x, \boldsymbol{\theta}), \\ u^k|_{\Gamma_+}(x, \boldsymbol{\theta}) &= \sum_{n=1}^k (-1)^{n-1} \frac{(x \cdot \boldsymbol{\theta})^n}{n!} u^{k-n}|_{\Gamma_+}(x, \boldsymbol{\theta}) + \frac{(-1)^k}{k!} I_a^k \mathbf{f}(x, \boldsymbol{\theta}), \quad \text{for } 1 \leq k \leq m. \end{aligned}$$

The inverse boundary value problem considered here seeks to recover the solution of the system (2.2a) and (2.2b) together with the unknown source \mathbf{f} from knowledge of $u^k|_{\Gamma \times \mathbb{S}^1}$, for all $k = 0, \dots, m$.

For specificity, we call $u^k(z, \boldsymbol{\theta})$ of (2.2) *the k -level flux*, for $k = 0, \dots, m$.

We use a Fourier approach, where functions u on $\Omega \times \mathbb{S}^1$ are characterized by the sequence valued map of their Fourier coefficients $u_{-n}(z) = \frac{1}{2\pi} \int_0^{2\pi} u(z, \boldsymbol{\theta}) e^{in\theta} d\theta$ (non-positive indexes are sufficient) in the angular variable,

$$\Omega \ni z \mapsto \mathbf{u}(z) := \langle u_0(z), u_{-1}(z), u_{-2}(z), \dots \rangle,$$

and work in the weighted l^2 spaces

$$(2.4) \quad l^{2, \frac{p}{2}}(\mathbb{N}; H^q(\Omega)) := \left\{ \mathbf{u} = \langle u_0, u_{-1}, u_{-2}, \dots \rangle : \|\mathbf{u}\|_{\frac{p}{2}, q}^2 := \sum_{j=0}^{\infty} (1+j)^p \|u_{-j}\|_{H^q(\Omega)}^2 < \infty \right\}$$

with traces $\mathbf{g} = \mathbf{u}|_{\Gamma} \in l^{2, \frac{p}{2}}(\mathbb{N}; H^{q-\frac{1}{2}}(\Gamma))$. The first (weight) index p refers to the smoothness in the angular variable, while the second index q shows the smoothness in the spatial variable.

Since \mathbf{f} vanishes on the lines outside Ω , we restrict $I_a^k \mathbf{f}$ to the lines intersecting $\bar{\Omega}$. These lines are parametrized by points on the boundary Γ and directions in \mathbb{S}^1 , yielding $I_a^k \mathbf{f}$ a function on the torus $\Gamma \times \mathbb{S}^1$. While Γ is also the unit circle, we keep the notation to differentiate from the set of directions. The maps in $l^{2, \frac{p}{2}}(\mathbb{N}; H^{q-\frac{1}{2}}(\Gamma))$ have a norm defined directly on the Fourier lattice

$$(2.5) \quad \|\mathbf{g}\|_{\frac{p}{2}, q-\frac{1}{2}}^2 = \sum_{j=0}^{\infty} \sum_{n=-\infty}^{\infty} (1+j)^p (1+|n|)^{2q-1} |g_{-j, n}|^2,$$

where $g_{-j, k} = \frac{1}{2\pi} \int_0^{2\pi} g_{-j}(e^{i\beta}) e^{-ik\beta} d\beta$, for $k \in \mathbb{Z}$, $j \geq 0$.

We use the notation $\|\mathbf{v}\| \lesssim \|\mathbf{w}\|$, whenever $\|\mathbf{v}\| \leq C \|\mathbf{w}\|$ for some constant $C > 0$ independent of \mathbf{v} and \mathbf{w} , and denote $\|\mathbf{v}\| \approx \|\mathbf{w}\|$ if $\|\mathbf{v}\| \lesssim \|\mathbf{w}\| \lesssim \|\mathbf{v}\|$.

Theorem 2.1. *Let Ω be the unit disc, $m \geq 1$ be an integer, and $a \in C^{m+1, \mu}(\bar{\Omega})$, $\mu > 1/2$. For some unknown real valued m -tensor $\mathbf{f} \in H_0^{m+\frac{3}{2}}(\mathbb{S}^m; \Omega)$, let $\mathbb{I}_a \mathbf{f} := \langle I_a^0 \mathbf{f}, I_a^1 \mathbf{f}, I_a^2 \mathbf{f}, \dots, I_a^m \mathbf{f} \rangle$ be the attenuated momenta ray transform as in (2.1). Then $I_a^k \mathbf{f} \in H^{m+\frac{3}{2}}(\mathbb{S}^1; H^{m+\frac{1}{2}}(\Gamma))$ for $0 \leq k \leq m$, and \mathbf{f} is determined by $\mathbb{I}_a \mathbf{f}$ with the estimate*

$$(2.6) \quad \|\mathbf{f}\|_{L^2(\Omega)}^2 \lesssim \sum_{j=0}^m \|I_a^j \mathbf{f}\|_{m+\frac{3}{2}, j+\frac{1}{2}}^2.$$

The method of proof is constructive.

3. A PRIORI ESTIMATES FOR SOLUTIONS OF INHOMOGENEOUS BUKHGEIM-BELTRAMI EQUATION

The stability estimate in Theorem 2.1 requires a priori estimates for solutions of the inhomogeneous Bukhgeim-Beltrami equation

$$(3.1) \quad \bar{\partial}\mathbf{v} + L^2\partial\mathbf{v} = \mathbf{w},$$

in the weighted spaces $l^{2, \frac{p}{2}}(\mathbb{N}; H^q(\Omega))$ for arbitrary positive integers p and q , where L denotes the left translation operator $L\mathbf{u} = L(u_0, u_{-1}, u_{-2}, \dots) := (u_{-1}, u_{-2}, \dots)$ and $\bar{\partial} = \frac{1}{2}(\partial_{x_1} + i\partial_{x_2})$, $\partial = \frac{1}{2}(\partial_{x_1} - i\partial_{x_2})$ are the Cauchy-Riemann operators.

Extension of the results in [15, Theorem 4.2] do not follow from differentiation of the equation, with the difficulty arising in the weighted estimates in p . They are due to the fact that the sequence valued maps $\Omega \ni z \mapsto (v_{-1}(z), 2^p v_{-2}(z), \dots, n^p v_{-n}(z), \dots)$ no longer solve a Beltrami equation of the type (3.1). However, a priori estimates of traces of higher order gradients of solution of (3.1) are necessary. To address this difficulty we first introduce a hierarchy of norms defined inductively for $p \geq 0$ integer as follows: On the set of sequences with elements in $H^q(\Omega)$, let $S^0(\mathbb{N}; H^q(\Omega))$ be the space of square summable sequences \mathbf{u} endowed with the norm

$$(3.2) \quad |||\mathbf{u}|||_{0,q} := \left(\sum_{j=0}^{\infty} \|u_j\|_{H^q(\Omega)}^2 \right)^{\frac{1}{2}},$$

and for $p \geq 1$, let

$$S^{\frac{p}{2}}(\mathbb{N}; H^q(\Omega)) := \left\{ \mathbf{u} = \langle u_0, u_{-1}, u_{-2}, \dots \rangle : |||\mathbf{u}|||_{\frac{p}{2},q} < \infty \right\},$$

where

$$(3.3) \quad |||\mathbf{u}|||_{\frac{p}{2},q} := \left(\sum_{n=0}^{\infty} |||L^n \mathbf{u}|||_{\frac{p-1}{2},q}^2 \right)^{\frac{1}{2}}.$$

The following result shows that the norm in (2.4) is equivalent to the one defined inductively above, yielding $S^{\frac{p}{2}}(\mathbb{N}; H^q(\Omega)) = l^{2, \frac{p}{2}}(\mathbb{N}; H^q(\Omega))$.

Lemma 3.1. *Let $|||\cdot|||_{\frac{p}{2},q}$ be the norm in (2.4) and $|||\cdot|||_{\frac{p}{2},q}$ be the norm defined inductively in (3.3), for some integers $p, q \geq 0$. Then*

$$(3.4) \quad |||\mathbf{u}|||_{\frac{p}{2},q} \approx |||\mathbf{u}|||_{\frac{p}{2},q}.$$

Proof. We first show by induction in p (and q fixed) the equality

$$(3.5) \quad |||\mathbf{u}|||_{\frac{p}{2},q}^2 = \sum_{j=0}^{\infty} C_p^{j+p} \|u_j\|_{H^q(\Omega)}^2,$$

where $C_p^{j+p} = \frac{(j+p)!}{j!p!}$.

The case $p = 0$ holds by definition (3.2).

Assume next that the equality in (3.5) holds for some fixed p .

By definition (3.3),

$$(3.6) \quad |||\mathbf{u}|||_{\frac{p+1}{2},q}^2 = \sum_{n=0}^{\infty} |||L^n \mathbf{u}|||_{\frac{p}{2},q}^2 = \sum_{m=0}^{\infty} \sum_{n=0}^{\infty} C_p^{m+p} \|u_{m+n}\|_{H^q(\Omega)}^2.$$

By changing the index $j = m + n$, for $m \geq 0$, ($j - n \geq 0$, and $n \leq j$) we get

$$(3.7) \quad \sum_{m=0}^{\infty} \sum_{n=0}^{\infty} C_p^{m+p} \|u_{m+n}\|_{H^q(\Omega)}^2 = \sum_{j=0}^{\infty} \sum_{n=0}^j C_p^{j-n+p} \|u_j\|_{H^q(\Omega)}^2 = \sum_{j=0}^{\infty} \|u_j\|_{H^q(\Omega)}^2 \sum_{n=0}^j C_p^{j-n+p}.$$

By using Pascal's recurrence and the telescopic cancellations,

$$\sum_{n=0}^j C_p^{j-n+p} = C_{p+1}^{j+p+1}.$$

Thus, from (3.7), $\|\mathbf{u}\|_{\frac{p+1}{2}, q}^2 = \sum_{j=0}^{\infty} C_{p+1}^{j+p+1} \|u_j\|_{H^q(\Omega)}^2$.

The equivalence of the norms in (3.4) follows from $\frac{1}{p!}(1+j)^p \leq C_p^{j+p} \leq (1+j)^p$. \square

The following result establishes the base case in the bootstrapping in the decay in p of solutions of (3.1).

Theorem 3.1. *Let $\mathbf{w} \in l^{2, \frac{p}{2}+1}(\mathbb{N}; L^2(\Omega))$ for some fixed integer $p \geq 0$. If $\mathbf{v} \in l^{2, \frac{p+1}{2}}(\mathbb{N}; H^1(\Omega))$ solves (3.1), then*

$$(3.8) \quad \|\mathbf{v}\|_{\frac{p}{2}, 1}^2 \lesssim \|\mathbf{w}\|_{\frac{p}{2}+1, 0}^2 + \|\mathbf{v}|_r\|_{\frac{p+1}{2}, \frac{1}{2}}^2.$$

Proof. We reason by induction in p . The case $p = 0$,

$$(3.9) \quad \|\mathbf{v}\|_{0, 1}^2 \lesssim \|\mathbf{w}\|_{1, 0}^2 + \|\mathbf{v}|_r\|_{\frac{1}{2}, \frac{1}{2}}^2,$$

is established in [15, Corollary 4.1].

Assume next that (3.8) holds for p :

$$(3.10) \quad \|\mathbf{v}\|_{\frac{p}{2}, 1}^2 \lesssim \|\mathbf{w}\|_{\frac{p}{2}+1, 0}^2 + \|\mathbf{v}|_r\|_{\frac{p+1}{2}, \frac{1}{2}}^2.$$

Next we bootstrap the decay in p in (3.10) by $\frac{1}{2}$. Since \mathbf{v} solves (3.1), for each $n \geq 0$, the left shifted sequence $L^n \mathbf{v}$ solves the shifted inhomogeneous Bukhgeim-Beltrami equation

$$(3.11) \quad \bar{\partial} L^n \mathbf{v} + L^2 \partial L^n \mathbf{v} = L^n \mathbf{w}.$$

Thus, it satisfies the estimate (3.10) with \mathbf{v} replaced by $L^n \mathbf{v}$, and \mathbf{w} replaced by $L^n \mathbf{w}$. A summation over n then yields

$$\sum_{n=0}^{\infty} \|L^n \mathbf{v}\|_{\frac{p}{2}, 1}^2 \lesssim \sum_{n=0}^{\infty} \|L^n \mathbf{w}\|_{\frac{p}{2}+1, 0}^2 + \sum_{n=0}^{\infty} \|L^n \mathbf{v}|_r\|_{\frac{p+1}{2}, \frac{1}{2}}^2,$$

which in view of the norm equivalence (3.4) rewrites as

$$(3.12) \quad \|\mathbf{v}\|_{\frac{p+1}{2}, 1}^2 \lesssim \|\mathbf{w}\|_{\frac{p+1}{2}+1, 0}^2 + \|\mathbf{v}|_r\|_{\frac{p+2}{2}, \frac{1}{2}}^2.$$

By hypothesis, the right-hand-side is finite. \square

For higher regularity estimates in the spatial variable, we need an estimate on the traces of higher order derivatives on the boundary. Suffices to consider the equation (3.1) away from the origin and work in polar coordinates.

Let $\Omega_\epsilon = \{\epsilon < |z| < 1\}$. In Ω_ϵ the Cauchy-Riemann operators rewrite in terms of the angular derivative ∂_η and the radial derivative ∂_r as

$$\partial = \frac{e^{-\eta}}{2} \left(\partial_r - \frac{1}{r} \partial_\eta \right) \quad \text{and} \quad \bar{\partial} = \frac{e^\eta}{2} \left(\partial_r + \frac{1}{r} \partial_\eta \right),$$

and the inhomogeneous Bukhgeim-Beltrami equation (3.1) becomes

$$(3.13) \quad A \partial_r \mathbf{v} = -\frac{1}{r} B \partial_\eta \mathbf{v} + 2e^\eta \mathbf{w}, \quad \epsilon < r < 1,$$

where

$$(3.14) \quad A := e^{2\eta} + L^2, \quad \text{and} \quad B := e^{2\eta} - L^2.$$

While it is easy to see that $A, B : l^{2,p}(\mathbb{N}; H^q(\Omega)) \rightarrow l^{2,p}(\mathbb{N}; H^q(\Omega))$ are bounded operators, they are not invertible on $l^{2,p}(\mathbb{N}; H^q(\Omega))$. The problem is that the unit circle lies in the spectrum of the left translation L^2 . However, A will be invertible on a proper subspace as follows. We start with a general result which may be of independent interest.

Lemma 3.2. *Let $p \geq 0$ be an integer, L be the left shift operator, and $\lambda \in \mathbb{C}$ with $|\lambda| \geq 1$. Let $\mathbf{a} \in l^{2,p}$ and $\mathbf{c} \in l^{2,p+1}$ be sequences satisfying $(\lambda + L^2)\mathbf{a} = \mathbf{c}$. Then*

$$\|\mathbf{a}\|_{l^{2,p}} \leq \frac{2^{p+1}}{2p+1} \|\mathbf{c}\|_{l^{2,p+1}}.$$

Proof. Since $a_j = \sum_{k=0}^{\infty} c_{j+2k} \lambda^{-k-1}$, suffices to show the stronger estimate

$$(3.15) \quad \left\{ \sum_{j=0}^{\infty} (1+j)^{2p} \left(\sum_{k=0}^{\infty} |c_{j+k}| \right)^2 \right\}^{\frac{1}{2}} \leq \frac{2^{p+1}}{(2p+1)} \left\{ \sum_{j=0}^{\infty} (1+j)^{2p+2} |c_j|^2 \right\}^{\frac{1}{2}}.$$

We prove first the continuous version:

$$\begin{aligned} & \left\{ \int_1^\infty (1+s)^{2p} \left(\int_s^\infty f(t) dt \right)^2 ds \right\}^{\frac{1}{2}} = \left\{ \int_1^\infty \left(\int_1^\infty s(1+s)^p f(s\zeta) d\zeta \right)^2 ds \right\}^{\frac{1}{2}} \\ & \leq 2^p \left\{ \int_1^\infty \left(\int_1^\infty s^{p+1} f(s\zeta) d\zeta \right)^2 ds \right\}^{\frac{1}{2}} \leq 2^p \int_1^\infty \left\{ \int_1^\infty s^{2p+2} f^2(s\zeta) ds \right\}^{\frac{1}{2}} d\zeta \\ & = 2^p \int_1^\infty \left\{ \int_\zeta^\infty \frac{t^{2p+2}}{\zeta^{2p+3}} f^2(t) dt \right\}^{\frac{1}{2}} d\zeta \leq 2^p \left\{ \int_1^\infty \zeta^{-p-\frac{3}{2}} d\zeta \right\} \left\{ \int_1^\infty t^{2p+2} f^2(t) dt \right\}^{\frac{1}{2}} \\ & \leq \frac{2^{p+1}}{2p+1} \left\{ \int_1^\infty (1+t)^{2p+2} f^2(t) dt \right\}^{\frac{1}{2}}, \end{aligned}$$

where the second inequality uses Minkowski's.

By setting $f(t) = |c_{[t]}|$, for $[t]$ the largest integer smaller than t , we obtain (3.15). \square

Proposition 3.1. *Let $p \geq 0$ be an integer, and A, B as in (3.14). Then for any integer $q \geq 0$,*

- (i) $A^{-1} : l^{2,p+q+1}(\mathbb{N}; H^q(\Omega_\epsilon)) \rightarrow l^{2,p}(\mathbb{N}; H^q(\Omega_\epsilon))$,
- (ii) $A^{-1} \frac{1}{r} B \partial_\eta : l^{2,p+q+1}(\mathbb{N}; H^{q+1}(\Omega_\epsilon)) \rightarrow l^{2,p}(\mathbb{N}; H^q(\Omega_\epsilon))$.

Proof of (i). The case $q = 0$ in (3.1) follows directly from Lemma 3.2 and an integration over Ω_ϵ .

Let $q \geq 1$ be arbitrarily fixed.

For any $\mathbf{c} \in l^{2,p+q+1}(\mathbb{N}; H^q(\Omega_\epsilon))$, we have

$$(3.16) \quad \left(\partial_r^\alpha A^{-1} \mathbf{c}(r, \eta) \right)_j = \sum_{k=0}^{\infty} \partial_r^\alpha c_{j+2k}(r, \eta) e^{-1(2k+1)\eta}, \quad 0 \leq \alpha \leq q.$$

An application of Lemma 3.2 and an integration over Ω_ϵ yields

$$(3.17) \quad \partial_r^\alpha A^{-1} : l^{2,p+1}(\mathbb{N}; H^q(\Omega_\epsilon)) \longrightarrow l^{2,p}(\mathbb{N}; H^{q-\alpha}(\Omega_\epsilon)).$$

For $0 \leq \beta \leq q$, by Leibniz formula,

$$\partial_\eta^\beta (A^{-1} \mathbf{c})_j = \sum_{s=0}^{\beta} (-1)^s C_s^\beta \sum_{k=0}^{\infty} \left(\partial_\eta^{\beta-s} c_{j+2k} \right) (2k+1)^s e^{-1(2k+1)\eta},$$

where $C_s^\beta = \frac{\beta!}{(\beta-s)!s!}$.

An integration over Ω_ϵ in

$$\begin{aligned} \sum_{j=0}^{\infty} (1+j)^{2p} |\partial_\eta^\beta (A^{-1} \mathbf{c})_j|^2 &\lesssim \sum_{s=0}^{\beta} \sum_{j=0}^{\infty} (1+j)^{2p} \left(\sum_{k=0}^{\infty} (k+1)^s |\partial_\eta^{\beta-s} c_{j+2k}| \right)^2 \\ &\lesssim \sum_{s=0}^{\beta} \left[\sum_{j=0}^{\infty} (1+j)^{2p} \left(\sum_{k=0}^{\infty} (1+j+k)^s |\partial_\eta^{\beta-s} c_{j+k}| \right)^2 \right] \\ &\lesssim \sum_{s=0}^{\beta} \sum_{j=0}^{\infty} (1+j)^{2p+2s+2} |\partial_\eta^{\beta-s} c_j|^2 \end{aligned}$$

(where the last inequality uses Lemma 3.2) yields

$$\|\partial_\eta^\beta A^{-1} \mathbf{c}\|_{p,0}^2 \lesssim \sum_{s=0}^{\beta} \|\partial_\eta^{\beta-s} \mathbf{c}\|_{p+s+1, q-\beta}^2.$$

Thus,

$$(3.18) \quad \partial_\eta^\beta A^{-1} : l^{2,p+q+1}(\mathbb{N}; H^q(\Omega_\epsilon)) \longrightarrow l^{2,p}(\mathbb{N}; H^{q-\beta}(\Omega_\epsilon)).$$

The mixed derivatives follow from (3.17) and (3.18) as well,

$$(3.19) \quad \partial_r^\alpha \partial_\eta^{q-\alpha} A^{-1} : l^{2,p+q+1}(\mathbb{N}; H^q(\Omega_\epsilon)) \longrightarrow l^{2,p}(\mathbb{N}; L^2(\Omega_\epsilon)),$$

thus yielding (3.1).

Proof of (ii): Since $\partial_\eta : l^{2,p}(\mathbb{N}; H^{q+1}(\Omega_\epsilon)) \longrightarrow l^{2,p}(\mathbb{N}; H^q(\Omega_\epsilon))$ and $B : l^{2,p}(\mathbb{N}; H^q(\Omega_\epsilon)) \longrightarrow l^{2,p}(\mathbb{N}; H^q(\Omega_\epsilon))$ are bounded, by part (i),

$$A^{-1} \frac{1}{r} B \partial_\eta : l^{2,p+q+1}(\mathbb{N}; H^{q+1}(\Omega_\epsilon)) \longrightarrow l^{2,p}(\mathbb{N}; H^q(\Omega_\epsilon)).$$

□

Estimates of higher regularity in the spatial variable use first an estimate on the traces of higher order derivatives at the boundary.

Corollary 3.1. *Let $\mathbf{w} \in l^{2, \frac{p}{2}+1}(\mathbb{N}; H^q(\Omega_\epsilon))$, for some $p \geq 0, q \geq 1$ integers. If $\mathbf{v} \in l^{2, \frac{p}{2}+1}(\mathbb{N}; H^{q+1}(\Omega_\epsilon))$ solves (3.1), then*

$$(3.20) \quad \|\nabla^q \mathbf{v}|_r\|_{\frac{p}{2}, \frac{1}{2}}^2 \lesssim \|\mathbf{v}|_r\|_{\frac{p}{2}+q+1, q+\frac{1}{2}}^2 + \|\mathbf{w}|_r\|_{\frac{p}{2}+q+1, q-\frac{1}{2}}^2,$$

where ∇ stands for either $\bar{\partial}$ or ∂ .

Proof. Recall (3.13):

$$A\partial_r \mathbf{v} = -\frac{1}{r}B\partial_\eta \mathbf{v} + 2e^m \mathbf{w},$$

with A, B as in (3.14).

By Proposition 3.1 (applying A^{-1} and $\partial_\eta^\beta \partial_r^\alpha$ with $\alpha + \beta + 1 = q$),

$$\partial_\eta^\beta \partial_r^\alpha \partial_r \mathbf{v} = -\partial_\eta^\beta \partial_r^\alpha A^{-1} \frac{1}{r} B \partial_\eta \mathbf{v} + 2\partial_\eta^\beta \partial_r^\alpha A^{-1} e^m \mathbf{w}$$

holds in $l^{2,p}(\mathbb{N}; H^1(\Omega_\epsilon))$. By taking the trace on Γ yields the estimate

$$(3.21) \quad \|\nabla^q \mathbf{v}|_r\|_{p, \frac{1}{2}}^2 \lesssim \|\mathbf{v}|_r\|_{p+q+1, q+\frac{1}{2}}^2 + \|\mathbf{w}|_r\|_{p+q+1, q-\frac{1}{2}}^2.$$

The estimate (3.21) is extended in the p index from non-negative integers to multiples of $\frac{1}{2}$ as follows.

Since $L^n \mathbf{v}$ solves the shifted inhomogeneous Bukhgeim-Beltrami equation (3.11), we can apply the estimate (3.21) with \mathbf{v} replaced by $L^n \mathbf{v}$ and \mathbf{w} replaced by $L^n \mathbf{w}$. A summation over n yields

$$(3.22) \quad \sum_{n=0}^{\infty} \|L^n \nabla^q \mathbf{v}|_r\|_{p, \frac{1}{2}}^2 \lesssim \sum_{n=0}^{\infty} \|L^n \mathbf{v}|_r\|_{p+q+1, q+\frac{1}{2}}^2 + \sum_{n=0}^{\infty} \|L^n \mathbf{w}|_r\|_{p+q+1, q-\frac{1}{2}}^2.$$

Each of the sums in the inequality (3.22) above are nothing else but the inductively defined norms (3.3). In conjunction with the norm equivalence (3.4), the inequality (3.22) rewrites:

$$\|\nabla^q \mathbf{v}|_r\|_{p+\frac{1}{2}, \frac{1}{2}}^2 \lesssim \|\mathbf{v}|_r\|_{p+q+\frac{3}{2}, q+\frac{1}{2}}^2 + \|\mathbf{w}|_r\|_{p+q+\frac{3}{2}, q-\frac{1}{2}}^2.$$

Since p was an arbitrary integer, this is the identity (3.20). \square

We are now able to prove a general interior estimate for solution of (3.1) in terms of their traces on the boundary. They are crucial in the bootstrapping argument.

Theorem 3.2. *Let $\mathbf{w} \in l^{2, \frac{p}{2}+q+\frac{3}{2}}(\mathbb{N}; H^q(\Omega))$ for some $p \geq 0$ and $q \geq 1$ integers. If $\mathbf{v} \in l^{2, \frac{p}{2}+q+\frac{3}{2}}(\mathbb{N}; H^{q+1}(\Omega))$ solves (3.1), then*

$$(3.23) \quad \|\mathbf{v}\|_{\frac{p}{2}, q+1}^2 \lesssim \|\mathbf{w}\|_{\frac{p}{2}+1, q}^2 + \|\mathbf{v}|_r\|_{\frac{p}{2}+q+\frac{3}{2}, q+\frac{1}{2}}^2 + \|\mathbf{w}|_r\|_{\frac{p}{2}+q+\frac{3}{2}, q-\frac{1}{2}}^2.$$

Proof. Since $\nabla^q \mathbf{v}$ solves

$$\bar{\partial}(\nabla^q \mathbf{v}) + L^2 \partial(\nabla^q \mathbf{v}) = \nabla^q \mathbf{w},$$

we apply Theorem 3.1 to $\nabla^q \mathbf{v}$:

$$\|\mathbf{v}\|_{\frac{p}{2}, q+1}^2 \lesssim \|\mathbf{w}\|_{\frac{p}{2}+1, q}^2 + \|\nabla^q \mathbf{v}|_r\|_{\frac{p}{2}+\frac{1}{2}, \frac{1}{2}}^2.$$

A further application of Corollary 3.1 to the last term establishes (3.23). \square

4. PROOF OF THEOREM 2.1 IN THE NON-ATTENUATED ($a = 0$) CASE

It is easy to see (e.g., in [34, Lemma A.1]) that

$$(4.1) \quad \langle \mathbf{f}, \boldsymbol{\theta}^m \rangle = \begin{cases} f_0 + \sum_{k=1}^{\frac{m}{2}} (f_{2k} e^{-1(2k)\theta} + f_{-2k} e^{1(2k)\theta}), & \text{if } m = \text{even}, \\ \sum_{k=0}^{\frac{m-1}{2}} (f_{2k+1} e^{-1(2k+1)\theta} + f_{-(2k+1)} e^{1(2k+1)\theta}), & \text{if } m = \text{odd}, \end{cases}$$

for some functions $\{f_k : -m \leq k \leq m\}$ in an explicit one-to-one correspondence (linear combination) with $\{\underbrace{f_1 \dots 1}_{m-k} \underbrace{2 \dots 2}_k : 0 \leq k \leq m\}$. For symmetric tensors, the latter coincide with $f_{i_1 \dots i_m}$ for all multi-indexes $(i_1, \dots, i_m) \in \{1, 2\}^m$ in which 2 occurs exactly k times.

We present the proof for the even order tensors, while for the odd order case we exhibit the nominal changes only.

Let m be an even integer and the attenuation $a \equiv 0$.

In our inverse problem, the solution v^k , $0 \leq k \leq m$ of the boundary value problem (2.2) with $a \equiv 0$ is unknown in Ω , since m -tensors \mathbf{f} is unknown. However, their traces

$$(4.2) \quad g^k = \begin{cases} v^k|_{\Gamma_+} & \text{on } \Gamma_+, \\ 0 & \text{on } \Gamma_-, \end{cases}$$

are known on $\Gamma \times \mathbb{S}^1$ from the momenta data $\langle I^0 \mathbf{f}, I^1 \mathbf{f}, \dots, I^m \mathbf{f} \rangle$ via (2.3) for $a \equiv 0$ therein:

$$(4.3) \quad \langle g^0, g^1, \dots, g^m \rangle \longleftrightarrow \langle I^0 \mathbf{f}, I^1 \mathbf{f}, \dots, I^m \mathbf{f} \rangle.$$

While unknown, by Proposition 2.1 the a priori smoothness assumption on \mathbf{f} yield $v^k \in H^{m+\frac{3}{2}}(\Omega \times \mathbb{S}^1)$. Thus $g^k, I^k \mathbf{f} \in H^{m+\frac{3}{2}}(\mathbb{S}^1; H^{m+\frac{1}{2}}(\Gamma))$ for $0 \leq k \leq m$.

For the inverse source problem we work with the sequence of the Fourier coefficients of the k -level flux $v^k(z, \cdot)$, in the angular variable:

$$(4.4) \quad v_n^k(z) = \frac{1}{2\pi} \int_{-\pi}^{\pi} v^k(z, \boldsymbol{\theta}) e^{-in\theta} d\theta, \quad n \in \mathbb{Z}, 0 \leq k \leq m.$$

The upper index k denotes the level of the flux, while the lower index n is the Fourier coefficient in the angular variable.

For $\theta = \arg \boldsymbol{\theta} \in (-\pi, \pi]$, the advection operator in polar coordinates becomes $\boldsymbol{\theta} \cdot \nabla = e^{-i\theta} \bar{\partial} + e^{i\theta} \partial$. By identifying the Fourier coefficients in (2.2) and by using (4.1), the modes v_n^k 's solve

$$(4.5a) \quad \bar{\partial} v_{-(2n-1)}^0(z) + \partial v_{-(2n+1)}^0(z) = f_{2n}(z), \quad 0 \leq n \leq m/2,$$

$$(4.5b) \quad \bar{\partial} v_{-(2n-1)}^0(z) + \partial v_{-(2n+1)}^0(z) = 0, \quad n \geq m/2 + 1,$$

$$(4.5c) \quad \bar{\partial} v_{-2n}^0(z) + \partial v_{-(2n+2)}^0(z) = 0, \quad n \geq 0,$$

$$(4.5d) \quad \bar{\partial} v_{-n}^k(z) + \partial v_{-n-2}^k(z) = v_{-n-1}^{k-1}(z), \quad n \in \mathbb{Z}, 1 \leq k \leq m,$$

and

$$(4.5e) \quad v_{-n}^k|_{\Gamma} = g_{-n}^k, \quad n \in \mathbb{Z}, 0 \leq k \leq m.$$

The existence of the solution to the boundary value problem (4.5) is postulated by the forward problem.

Since \mathbf{f} is real valued, the solution v^k of (2.2) is also real valued, and its Fourier modes in the angular variable occur in conjugates:

$$(4.6) \quad v_{-n}^k = \overline{v_n^k}, \quad \text{for } n \geq 0, 0 \leq k \leq m.$$

Thus, it suffices to consider the non-positive Fourier modes of $v^k(z, \cdot)$.

For $0 \leq k \leq m$, let \mathbf{v}^k be the sequence valued map of the non-positive Fourier coefficients of the solution v^k and \mathbf{g}^k be its corresponding trace on the boundary:

$$(4.7) \quad \mathbf{v}^k(z) := \langle v_0^k(z), v_{-1}^k(z), v_{-2}^k(z), \dots \rangle, \quad z \in \Omega,$$

$$(4.8) \quad \mathbf{g}^k = \langle g_0^k, g_{-1}^k, g_{-2}^k, \dots \rangle := \mathbf{v}^k|_\Gamma.$$

In the sequence valued map notation the boundary value problem (4.5) becomes

$$(4.9a) \quad \overline{\partial} v_{-1}^0 + \partial v_{-1}^0 = f_0,$$

$$(4.9b) \quad \overline{\partial} \mathbf{v}^0 + L^2 \partial \mathbf{v}^0 = L\mathbf{F},$$

$$(4.9c) \quad \overline{\partial} \mathbf{v}^k + L^2 \partial \mathbf{v}^k = L\mathbf{v}^{k-1}, \quad 1 \leq k \leq m,$$

subject to

$$(4.9d) \quad \mathbf{v}^k|_\Gamma = \mathbf{g}^k, \quad \text{for } 0 \leq k \leq m,$$

where

$$(4.10) \quad \mathbf{F} := \langle f_0, 0, f_2, 0, f_4, 0, \dots, f_{m-2}, 0, f_m, 0, 0, \dots \rangle$$

is the sequence valued map build on the Fourier modes $\{f_{2k} : 0 \leq k \leq \frac{m}{2}\}$ in (4.1) for $m = \text{even}$.

Note that the sequences \mathbf{v}^k , $0 \leq k \leq m$ in (4.9) are unknown, since \mathbf{F} is unknown. However, their traces on Γ are known from (4.3).

It is crucial to note that $L^{m+1}\mathbf{F} = \mathbf{0} = \langle 0, 0, \dots \rangle$, so that for $0 \leq k \leq m$, $L^{m-k}\mathbf{v}^k$ solves the boundary value problem

$$(4.11a) \quad \overline{\partial}[L^m \mathbf{v}^0] + L^2 \partial[L^m \mathbf{v}^0] = \mathbf{0},$$

$$(4.11b) \quad \overline{\partial}[L^{m-k} \mathbf{v}^k] + L^2 \partial[L^{m-k} \mathbf{v}^k] = L^{m-k+1} \mathbf{v}^{k-1}, \quad 1 \leq k \leq m,$$

subject to

$$(4.11c) \quad L^{m-k} \mathbf{v}^k|_\Gamma = L^{m-k} \mathbf{g}^k, \quad 0 \leq k \leq m,$$

which does not involve the source \mathbf{F} (encoding the tensor)!

The following result identifies shifts of the solutions of the boundary value problem (4.9) which are determined solely from the boundary data $\langle \mathbf{g}^0, \mathbf{g}^1, \dots, \mathbf{g}^m \rangle$ as in (4.8) and not by the source \mathbf{F} .

Proposition 4.1. *Let $\langle \mathbf{g}^0, \mathbf{g}^1, \dots, \mathbf{g}^m \rangle$ be the data as in (4.8) obtained for some unknown even order m -tensor in $H_0^{m+\frac{3}{2}}(\mathbf{S}^m; \Omega)$. Then $\mathbf{g}^k \in l^{2, m+\frac{3}{2}}(\mathbb{N}; H^{m+\frac{1}{2}}(\Gamma))$, and the unique solution \mathbf{v}^k of the boundary value problem (4.9) satisfies*

$$(4.12) \quad L^{m-k} \mathbf{v}^k(z) = \sum_{j=0}^k \mathcal{T}^j L^{m-k+j} [\mathcal{B} \mathbf{g}^{k-j}](z), \quad z \in \Omega, 0 \leq k \leq m,$$

where \mathcal{B} is the Bukhgeim-Cauchy operator in (B.3), and \mathcal{T} is the operator in (B.5). Moreover,

$$(4.13) \quad \|L^{m-k} \mathbf{v}^k\|_{m-k, k+1}^2 \lesssim \sum_{j=0}^k \|L^{m-j} \mathbf{g}^j\|_{m+\frac{3}{2}, j+\frac{1}{2}}^2, \quad 0 \leq k \leq m.$$

Proof. The existence of the solution to the boundary value problem (4.9) is postulated by the forward problem (2.2) (with $a \equiv 0$). Moreover, by Proposition 2.1, the unknown k -level flux $v^k \in H^{m+\frac{3}{2}}(\mathbb{S}^1; H^{m+1}(\Omega))$, yielding $\mathbf{v}^k \in l^{2, m+\frac{3}{2}}(\mathbb{N}; H^{m+1}(\Omega))$ and $\mathbf{g}^k \in l^{2, m+\frac{3}{2}}(\mathbb{N}; H^{m+\frac{1}{2}}(\Gamma))$.

Recall that $L^{m-k}\mathbf{v}^k$ solve the system (4.11).

First we prove the formula (4.12) with estimate (4.13) by induction in k , for $0 \leq k \leq m$.

Case $k = 0$: Since $L^m\mathbf{v}^0$ is L^2 -analytic, the Bukhgeim-Cauchy Integral formula (B.3) determines the sequence $L^m\mathbf{v}^0$ inside Ω from its boundary values via

$$(4.14) \quad L^m\mathbf{v}^0(z) := \mathcal{B}L^m\mathbf{g}^0(z), \quad z \in \Omega.$$

Applying Theorem 3.1 to the boundary value problem (4.11a) and (4.11c) yields

$$(4.15) \quad \|L^m\mathbf{v}^0\|_{m,1}^2 \lesssim \|L^m\mathbf{g}^0\|_{m+\frac{1}{2},\frac{1}{2}}^2,$$

thus showing the $k = 0$ case.

Next, we assume (4.12) and (4.13) holds for k :

$$(4.16) \quad L^{m-k}\mathbf{v}^k(z) = \sum_{j=0}^k \mathcal{T}^j L^{m-k+j}[\mathcal{B}\mathbf{g}^{k-j}](z), \quad z \in \Omega,$$

satisfies

$$(4.17) \quad \|L^{m-k}\mathbf{v}^k\|_{m-k,k+1}^2 \lesssim \sum_{j=0}^k \|L^{m-j}\mathbf{g}^j\|_{m+\frac{3}{2},j+\frac{1}{2}}^2,$$

and prove it for $k + 1$.

Starting from equation (4.11b) and (4.11c) for $k + 1$, $L^{m-(k+1)}\mathbf{v}^{k+1}$ solves

$$(4.18a) \quad \bar{\partial}[L^{m-(k+1)}\mathbf{v}^{k+1}] + L^2\partial[L^{m-(k+1)}\mathbf{v}^{k+1}] = L^{m-k}\mathbf{v}^k,$$

subject to

$$(4.18b) \quad L^{m-(k+1)}\mathbf{v}^{k+1}|_{\Gamma} = L^{m-(k+1)}\mathbf{g}^{k+1}.$$

Applying Proposition B.1 to (4.18), the solution $L^{m-(k+1)}\mathbf{v}^{k+1}$ is given by (B.6):

$$L^{m-(k+1)}\mathbf{v}^{k+1} = \mathcal{B}L^{m-(k+1)}\mathbf{g}^{k+1} + \mathcal{T}(L^{m-k}\mathbf{v}^k).$$

Following directly from their definitions, the operators L and \mathcal{B} commute, and the operators L and \mathcal{T} commute. Using these commuting properties and the induction hypothesis (4.16) yields

$$\begin{aligned} L^{m-(k+1)}\mathbf{v}^{k+1} &= L^{m-(k+1)}[\mathcal{B}\mathbf{g}^{k+1}] + \mathcal{T}(L^{m-k}\mathbf{v}^k) \\ &= L^{m-(k+1)}[\mathcal{B}\mathbf{g}^{k+1}] + \sum_{j=0}^k \mathcal{T}^{j+1}L^{m-k+j}[\mathcal{B}\mathbf{g}^{k-j}] = \sum_{j=0}^{k+1} \mathcal{T}^j L^{m-(k+1)+j}[\mathcal{B}\mathbf{g}^{k+1-j}]. \end{aligned}$$

This finished the inductive step of (4.16).

Next, we show the induction step for the estimate (4.17) for the solution $L^{m-(k+1)}\mathbf{v}^{k+1}$ of (4.18).

By applying Theorem 3.2 to (4.18) yields

$$\begin{aligned}
\|L^{m-k-1}\mathbf{v}^{k+1}\|_{m-k-1,k+2}^2 &\lesssim \|L^{m-k}\mathbf{v}^k\|_{m-k,k+1}^2 + \|L^{m-k}\mathbf{v}^k|_\Gamma\|_{m+\frac{3}{2},k+\frac{1}{2}}^2 + \|L^{m-k-1}\mathbf{v}^{k+1}|_\Gamma\|_{m+\frac{3}{2},k+\frac{3}{2}}^2 \\
&\lesssim \sum_{j=0}^k \|L^{m-j}\mathbf{v}^j|_\Gamma\|_{m+\frac{3}{2},j+\frac{1}{2}}^2 + \|L^{m-k-1}\mathbf{v}^{k+1}|_\Gamma\|_{m+\frac{3}{2},k+\frac{3}{2}}^2 \\
&\lesssim \sum_{j=0}^{k+1} \|L^{m-j}\mathbf{g}^j\|_{m+\frac{3}{2},j+\frac{1}{2}}^2,
\end{aligned}$$

where the second inequality uses the induction hypothesis (4.17), while the last one is regrouping. \square

4.1. The reconstruction method. We reconstruct the m -tensors \mathbf{f} by first recovering \mathbf{v}^k , $0 \leq k \leq m$ in two steps, see Figure 1.

- Step I (Sweep down):

Level by level, starting from $k = 0$ to $k = m$, we recover $L^{m-k}\mathbf{v}^k$ by solving the boundary value problem

$$\bar{\partial}(L^{m-k}\mathbf{v}^k) + L^2\partial(L^{m-k}\mathbf{v}^k) = L^{m+1-k}\mathbf{v}^{k-1}, \quad 1 \leq k \leq m,$$

subject to

$$L^{m-k}\mathbf{v}^k|_\Gamma = L^{m-k}\mathbf{g}^k, \quad \text{for } 1 \leq k \leq m.$$

Proposition 4.1 ensures that the unique solution $L^{m-k}\mathbf{v}^k$ given by (4.12) satisfies estimate (4.13). In particular, when $k = m$, the entire sequence \mathbf{v}^m (not just some translation of it) is recovered from the data \mathbf{g}^j , $0 \leq j \leq m$,

$$(4.19) \quad \mathbf{v}^m(z) = \sum_{j=0}^m [\mathcal{T}L]^j (\mathcal{B}\mathbf{g}^{m-j})(z), \quad z \in \Omega,$$

with the estimate

$$(4.20) \quad \|\mathbf{v}^m\|_{0,m+1}^2 \lesssim \sum_{j=0}^m \|L^{m-j}\mathbf{g}^j\|_{m+\frac{3}{2},j+\frac{1}{2}}^2;$$

where \mathcal{B} and \mathcal{T} are the operators in (B.3), respectively in (B.5).

- Step II (Sweep up):

Level by level, starting from $k = m$ to $k = 1$, use (4.9c) in its component-wise form (4.5d),

$$(4.21) \quad v_{-n-1}^{k-1} := \bar{\partial}v_{-n}^k + \partial v_{-n-2}^k, \quad n \geq 0,$$

to recover $L\mathbf{v}^{k-1}$ from the knowledge of \mathbf{v}^k .

Moreover, repeated differentiation of (4.21) yields

$$\nabla^q(L\mathbf{v}^{k-1}) = \bar{\partial}[\nabla^q\mathbf{v}^k] + L^2\partial[\nabla^q\mathbf{v}^k], \quad q \geq 1,$$

with the estimate

$$(4.22) \quad \|L\mathbf{v}^{k-1}\|_{0,q}^2 \lesssim \|\mathbf{v}^k\|_{0,q+1}^2.$$

We use (4.21) recursively to recover the entire sequences $\mathbf{v}^{m-1}, \dots, \mathbf{v}^1, \mathbf{v}^0$ with estimate

$$(4.23) \quad \|L\mathbf{v}^0\|_{0,1}^2 \lesssim \|\mathbf{v}^m\|_{0,m+1}^2.$$

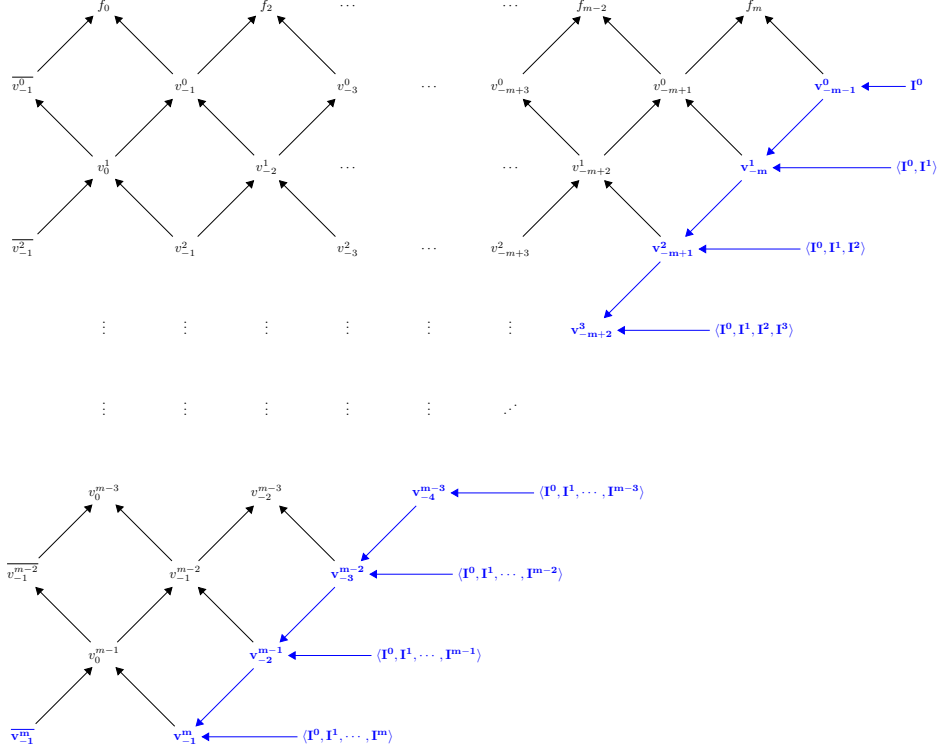


FIGURE 1. Flow of the reconstruction of even order tensors. In the sweep down, all the modes colored in blue are determined layer by layer from the momenta ray data and the previous layer. In the sweep up, also layer by layer starting from the bottom, the remaining coefficients are recovered. The arrows indicate which modes determine what.

- The reconstruction of the m -tensors \mathbf{f} .

With \mathbf{v}^0 known, we recover \mathbf{F} via (4.9b) and (4.9a),

$$(4.24) \quad f_0 := 2 \operatorname{Re} [\partial v_{-1}^0], \quad \text{and} \quad L\mathbf{F} := \bar{\partial}\mathbf{v}^0 + L^2\partial\mathbf{v}^0.$$

Moreover, using in order (4.24), (4.23) and (4.20), we have the estimate

$$(4.25) \quad \|\mathbf{F}\|_{0,0}^2 \lesssim \|\mathbf{v}^0\|_{0,1}^2 \lesssim \|\mathbf{v}^m\|_{0,m+1}^2 \lesssim \sum_{j=0}^m \|L^{m-j}\mathbf{g}^j\|_{m+\frac{3}{2},j+\frac{1}{2}}^2.$$

Finally, the components $f_{i_1 \dots i_m} = \underbrace{f_1 \dots 1}_{m-k} \underbrace{2 \dots 2}_k$ are defined via the explicit one-to-one correspondence (linear combination) with $\{f_{2k} : -m/2 \leq k \leq m/2\}$.

Since $\|\mathbf{f}\|_{L^2(\Omega)}^2 \lesssim \|\mathbf{F}\|_{0,0}^2 \lesssim \|\mathbf{f}\|_{L^2(\Omega)}^2$, Theorem 2.1 is, thus, proven for m even and $a \equiv 0$. \square

The proof of Theorem 2.1 for odd m -order tensors follows similarly to the even case with some nominal changes: As before, let \mathbf{v}^k be the sequence valued map of the Fourier coefficients of the k -level flux solution v^k of the boundary value problem (2.2) (with $a \equiv 0$) and $\mathbf{g}^k = \mathbf{v}^k|_F$ be its trace. Then \mathbf{v}^k solves (contrast with the system (4.9))

$$(4.26a) \quad \bar{\partial}\mathbf{v}^0 + L^2\partial\mathbf{v}^0 = L\mathbf{F},$$

$$(4.26b) \quad \bar{\partial}\mathbf{v}^k + L^2\partial\mathbf{v}^k = L\mathbf{v}^{k-1}, \quad 1 \leq k \leq m,$$

subject to

$$(4.26c) \quad \mathbf{v}^k|_\Gamma = \mathbf{g}^k, \quad \text{for } 0 \leq k \leq m,$$

where

$$(4.26d) \quad \mathbf{F} := \langle 0, f_1, 0, f_3, 0, f_4, 0, \dots, f_{m-2}, 0, f_m, 0, 0, \dots \rangle$$

is build on the Fourier modes $\{f_{2k+1} : 0 \leq k \leq \frac{m-1}{2}\}$ in (4.1) for $m = \text{odd}$. Note also the change in the definition of \mathbf{F} above from the one in the even tensor case in (4.10).

Proposition 4.1 holds verbatim for odd m .

Following the two step reconstruction method in the even case, \mathbf{F} and thus \mathbf{f} are similarly recovered with the estimate (2.6). The inversion of the momenta Doppler transform ($m = 1$) is detailed in the numerical section 6.

5. PROOF OF THEOREM 2.1 IN THE ATTENUATED CASE

As in [32] we treat the attenuated case by the reduction to the non-attenuated case via the special integrating factor function introduced in [14]:

$$h(z, \boldsymbol{\theta}) := \int_0^\infty a(z + t\boldsymbol{\theta}) dt - \frac{1}{2} (I - {}_1H) Ra(z \cdot \boldsymbol{\theta}^\perp, \boldsymbol{\theta}^\perp),$$

where $H\psi(s, \boldsymbol{\theta}) = \frac{1}{\pi} \int_{-\infty}^\infty \frac{\psi(t, \boldsymbol{\theta})}{s-t} dt$ is the Hilbert transform taken in the linear variable, and $Ra(s, \boldsymbol{\theta}^\perp) = \int_{-\infty}^\infty a(s\boldsymbol{\theta}^\perp + t\boldsymbol{\theta}) dt$ is the Radon transform of a .

It is known that all the negative Fourier modes of h vanish [14, 27], yielding

$$e^{-h(z, \boldsymbol{\theta})} := \sum_{k=0}^\infty \alpha_k(z) e^{ik\boldsymbol{\theta}}, \quad e^{h(z, \boldsymbol{\theta})} := \sum_{k=0}^\infty \beta_k(z) e^{ik\boldsymbol{\theta}}, \quad (z, \boldsymbol{\theta}) \in \overline{\Omega} \times \mathbb{S}^1.$$

In [15], the convolution operators $e^{\pm G}$ are defined by

$$(5.1) \quad e^{-G}\mathbf{u} := \boldsymbol{\alpha} * \mathbf{u} \text{ and } e^G\mathbf{u} := \boldsymbol{\beta} * \mathbf{u}, \text{ where } \boldsymbol{\alpha} := \langle \alpha_0, \alpha_1, \dots \rangle, \boldsymbol{\beta} := \langle \beta_0, \beta_1, \dots \rangle.$$

The following result connecting the attenuated to the non-attenuated case is a slight generalization of [15, Lemma 2.2].

Lemma 5.1. *Let $a \in C^{1,\mu}(\overline{\Omega})$, $\mu > 1/2$. Then $e^{\pm G} : l^{2,p}(\mathbb{N}; H^q(\Omega)) \rightarrow l^{2,p}(\mathbb{N}; H^q(\Omega))$ are bounded. Moreover,*

(i) *if $\mathbf{u} \in l^2(\mathbb{N}; H^1(\Omega))$ solves $\bar{\partial}\mathbf{u} + L^2\partial\mathbf{u} + aL\mathbf{u} = \mathbf{w}$, then $\mathbf{v} = e^{-G}\mathbf{u} \in l^2(\mathbb{N}; H^1(\Omega))$ solves $\bar{\partial}\mathbf{v} + L^2\partial\mathbf{v} = e^{-G}\mathbf{w}$;*

(ii) *Conversely, if $\mathbf{v} \in l^2(\mathbb{N}; H^1(\Omega))$ solves $\bar{\partial}\mathbf{v} + L^2\partial\mathbf{v} = e^{-G}\mathbf{w}$, then $\mathbf{u} = e^G\mathbf{v} \in l^2(\mathbb{N}; H^1(\Omega))$ solves $\bar{\partial}\mathbf{u} + L^2\partial\mathbf{u} + aL\mathbf{u} = \mathbf{w}$.*

The mapping properties of $e^{\pm G}$ and the case $\mathbf{w} = \mathbf{0}$ in (i) and (ii) are proven in [15]. The case $\mathbf{w} \neq \mathbf{0}$ follows similarly. □

Below we prove Theorem 2.1 in the attenuated case for even order tensors. The proof for the odd order tensors follows similarly.

Let m be an even integer and attenuation $a \in C^{m+1,\mu}(\overline{\Omega})$, $\mu > 1/2$.

In our inverse problem, the k -level flux solution u^k , $0 \leq k \leq m$ of the boundary value problem (2.2) is unknown in Ω , since m -tensors \mathbf{f} is unknown. However, their traces

$$(5.2) \quad g^k = \begin{cases} u^k|_{\Gamma_+} & \text{on } \Gamma_+, \\ 0 & \text{on } \Gamma_-, \end{cases}$$

are known on $\Gamma \times \mathbb{S}^1$ from the momenta data $\langle I_a^0 \mathbf{f}, I_a^1 \mathbf{f}, \dots, I_a^m \mathbf{f} \rangle$ via (2.3):

$$(5.3) \quad \langle g^0, g^1, \dots, g^m \rangle \longleftrightarrow \langle I_a^0 \mathbf{f}, I_a^1 \mathbf{f}, \dots, I_a^m \mathbf{f} \rangle.$$

While unknown, by Proposition 2.1 the a priori smoothness assumption on m -tensors \mathbf{f} and attenuation a yield $u^k \in H^{m+\frac{3}{2}}(\Omega \times \mathbb{S}^1)$. Thus $g^k, I_a^k \mathbf{f} \in H^{m+\frac{3}{2}}(\mathbb{S}^1; H^{m+\frac{1}{2}}(\Gamma))$ for $0 \leq k \leq m$.

For $0 \leq k \leq m$, let $\mathbf{u}^k = \langle u_0^k, u_{-1}^k, u_{-2}^k, \dots \rangle$ be the sequence valued map of the Fourier coefficients of u^k in the angular variable, and $\mathbf{g}^k = \mathbf{u}^k|_{\Gamma}$ be its corresponding trace on the boundary.

By identifying the same order modes in (2.2), \mathbf{u}^k solves

$$(5.4a) \quad \overline{\partial} u_{-1}^0 + \partial u_{-1}^0 + a u_0^0 = f_0,$$

$$(5.4b) \quad \overline{\partial} \mathbf{u}^0 + L^2 \partial \mathbf{u}^0 + a L \mathbf{u}^0 = L \mathbf{F},$$

$$(5.4c) \quad \overline{\partial} \mathbf{u}^k + L^2 \partial \mathbf{u}^k + a L \mathbf{u}^k = L \mathbf{u}^{k-1}, \quad 1 \leq k \leq m,$$

subject to

$$(5.4d) \quad \mathbf{g}^k = \mathbf{u}^k|_{\Gamma}, \quad \text{for } 0 \leq k \leq m,$$

where \mathbf{F} is as defined in (4.10).

The existence of the solution to the boundary value problem (5.4) is postulated by the forward problem. By Proposition 2.1, the k -level flux $u^k \in H^{m+\frac{3}{2}}(\mathbb{S}^1; H^{m+1}(\Omega))$. Thus, the sequences $\mathbf{u}^k \in l^{2, m+\frac{3}{2}}(\mathbb{N}; H^{m+1}(\Omega))$ and $\mathbf{g}^k \in l^{2, m+\frac{3}{2}}(\mathbb{N}; H^{m+\frac{1}{2}}(\Gamma))$.

For e^{-G} as in (5.1), define

$$(5.5) \quad \mathbf{v}^k := e^{-G} \mathbf{u}^k, \quad \text{for } 0 \leq k \leq m.$$

By Lemma 5.1, $\mathbf{v}^k \in l^{2, m+1}(\mathbb{N}; H^{m+1}(\Omega))$, $\mathbf{v}^k|_{\Gamma} \in l^{2, m+1}(\mathbb{N}; H^{m+1/2}(\Gamma))$, and \mathbf{v}^k solves

$$(5.6a) \quad \overline{\partial} v_{-1}^0 + \partial v_{-1}^0 = (e^{-G} \mathbf{F})_0,$$

$$(5.6b) \quad \overline{\partial} \mathbf{v}^0 + L^2 \partial \mathbf{v}^0 = L[e^{-G} \mathbf{F}],$$

$$(5.6c) \quad \overline{\partial} \mathbf{v}^k + L^2 \partial \mathbf{v}^k = L \mathbf{v}^{k-1}, \quad 1 \leq k \leq m,$$

subject to

$$(5.6d) \quad \mathbf{v}^k|_{\Gamma} = e^{-G} \mathbf{g}^k, \quad \text{for } 0 \leq k \leq m.$$

Note that $L^{m+1} \mathbf{F} = \mathbf{0} = \langle 0, 0, \dots \rangle$. Since $e^{\pm G}$ and L commute,

$$L^{m+1}[e^{-G} \mathbf{F}] = e^{-G} L^{m+1} \mathbf{F} = e^{-G} \mathbf{0} = \mathbf{0}.$$

Thus, $L^{m-k} \mathbf{v}^k$ solve

$$(5.7a) \quad \overline{\partial}[L^m \mathbf{v}^0] + L^2 \partial[L^m \mathbf{v}^0] = \mathbf{0},$$

$$(5.7b) \quad \overline{\partial}[L^{m-k} \mathbf{v}^k] + L^2 \partial[L^{m-k} \mathbf{v}^k] = L^{m-k+1} \mathbf{v}^{k-1}, \quad 1 \leq k \leq m,$$

subject to

$$(5.7c) \quad L^{m-k} \mathbf{v}^k|_{\Gamma} = e^{-G} L^{m-k} \mathbf{g}^k, \quad 0 \leq k \leq m.$$

Since the attenuation a is known and the sequences in (5.4d) are known on Γ from (5.3), the sequences $e^{-G}\mathbf{g}^k$ in (5.6d) are also determined.

Proposition 4.1 with \mathbf{g} replaced by $e^{-G}\mathbf{g}$ therein yields:

Proposition 5.1. *For $a \in C^{m+1,\mu}(\bar{\Omega})$, $\mu > 1/2$ given, let $\langle \mathbf{g}^0, \mathbf{g}^1, \dots, \mathbf{g}^m \rangle$ be the data as in (5.4d) obtained for some unknown even order m -tensor in $H_0^{m+\frac{3}{2}}(\mathbf{S}^m; \Omega)$. Then $\mathbf{g}^k \in l^{2,m+\frac{3}{2}}(\mathbb{N}; H^{m+\frac{1}{2}}(\Gamma))$, and the unique solution \mathbf{v}^k of the boundary value problem (5.6) satisfies*

$$L^{m-k}\mathbf{v}^k(z) = \sum_{j=0}^k \mathcal{T}^j L^{m-k+j} [\mathcal{B}e^{-G}\mathbf{g}^{k-j}](z), \quad z \in \Omega, \quad 0 \leq k \leq m,$$

where \mathcal{B}, \mathcal{T} are the operators in (B.3), respectively (B.5), and $e^{\pm G}$ are the operators in (5.1). Moreover,

$$\|L^{m-k}\mathbf{v}^k\|_{m-k,k+1}^2 \lesssim \sum_{j=0}^k \|e^{-G}L^{m-j}\mathbf{g}^j\|_{m+\frac{3}{2},j+\frac{1}{2}}^2, \quad 0 \leq k \leq m.$$

The reconstruction method of the non-attenuated case recovers $e^{-G}\mathbf{F}$ via (5.6a) and (5.6b):

$$(e^{-G}\mathbf{F})_0 := 2 \operatorname{Re} [\partial v_{-1}^0] \quad \text{and} \quad L[e^{-G}\mathbf{F}] := \bar{\partial}\mathbf{v}^0 + L^2\partial\mathbf{v}^0,$$

with the estimate $\|e^{-G}\mathbf{F}\|_{0,0}^2 \lesssim \sum_{j=0}^m \|e^{-G}L^{m-j}\mathbf{g}^j\|_{m+\frac{3}{2},j+\frac{1}{2}}^2$.

Since $\mathbf{F} = e^G [e^{-G}\mathbf{F}]$, an application of Lemma 5.1 yields $\|\mathbf{F}\|_{0,0}^2 \lesssim \sum_{j=0}^m \|L^{m-j}\mathbf{g}^j\|_{m+\frac{3}{2},j+\frac{1}{2}}^2$. \square

6. NUMERICAL INVERSION OF THE MOMENTA DOPPLER TRANSFORM

In this section we apply the reconstruction method to three numerical examples in the case $m = 1$ and $a \equiv 0$. Since the odd tensor case was not detailed in Section 4, we do it here in the Doppler case. Specifically, a vector field $\mathbf{f} = \langle F_1, F_2 \rangle$ is to be determined from its Doppler transform

$$(6.1) \quad I^0\mathbf{f}(x, \boldsymbol{\theta}) = \int_{-\infty}^{\infty} \boldsymbol{\theta} \cdot \mathbf{f}(\Pi_{\boldsymbol{\theta}}(x) + t\boldsymbol{\theta}) dt,$$

and its first-moment-Doppler transform

$$(6.2) \quad I^1\mathbf{f}(x, \boldsymbol{\theta}) = \int_{-\infty}^{\infty} t\boldsymbol{\theta} \cdot \mathbf{f}(\Pi_{\boldsymbol{\theta}}(x) + t\boldsymbol{\theta}) dt, \quad (x, \boldsymbol{\theta}) \in \mathbb{R}^2 \times \mathbb{S}^1,$$

where I^0 and I^1 are the ray transform as in (2.1).

For $k = 0, 1$, let v^k be the k -level flux solution of the boundary value problem (2.2).

In our inverse problem, the solution (v^0, v^1) is unknown in Ω , since \mathbf{f} is unknown. However, from the momenta Doppler data $\langle I^0\mathbf{f}, I^1\mathbf{f} \rangle$, their traces $g^k = \begin{cases} v^k|_{\Gamma_+} & \text{on } \Gamma_+, \\ 0 & \text{on } \Gamma_-, \end{cases}$ are determined via (2.3):

$$(6.3) \quad \langle g^0, g^1 \rangle \longleftrightarrow \langle I^0\mathbf{f}, I^1\mathbf{f} \rangle.$$

By identifying the Fourier coefficients in (2.2), the solution v_n^k 's solve

$$(6.4a) \quad \bar{\partial}v_0^0(z) + \partial v_{-2}^0(z) = f_1(z),$$

$$(6.4b) \quad \bar{\partial}v_{-n}^0(z) + \partial v_{-n-2}^0(z) = 0, \quad n \geq 1,$$

$$(6.4c) \quad \bar{\partial}v_{-n}^1(z) + \partial v_{-n-2}^1(z) = v_{-n-1}^0(z), \quad n \in \mathbb{Z},$$

and

$$(6.4d) \quad v_{-n}^k|_\Gamma = g_{-n}^k, \quad k = 0, 1,$$

where

$$(6.4e) \quad f_1 := \frac{1}{2}(F_1 + {}_1F_2).$$

Since the vector field \mathbf{f} is real valued, the solution v^k of (2.2) is also real valued, and its Fourier modes v_{-n}^k 's in the angular variable occur in conjugates:

$$(6.5) \quad v_n^k = \overline{v_{-n}^k}, \quad \text{for } n \geq 0, k = 0, 1.$$

Thus, it suffices to consider the non-positive Fourier modes of v^k .

As before, let \mathbf{v}^k be the sequence valued map of the non-positive Fourier coefficients of v^k , and $\mathbf{g}^k = \mathbf{v}^k|_\Gamma$ be its trace. Then in the sequence valued map notation the boundary value problem (6.4) becomes

$$(6.6a) \quad \bar{\partial}v_0^0 + \partial v_{-2}^0 = f_1,$$

$$(6.6b) \quad \bar{\partial}[L\mathbf{v}^0] + L^2\partial[L\mathbf{v}^0] = \mathbf{0},$$

$$(6.6c) \quad \bar{\partial}\mathbf{v}^1 + L^2\partial\mathbf{v}^1 = L\mathbf{v}^0,$$

subject to

$$(6.6d) \quad \mathbf{v}^k|_\Gamma = \mathbf{g}^k, \quad \text{for } k = 0, 1.$$

Note that the sequences $\langle \mathbf{v}^0, \mathbf{v}^1 \rangle$ of the boundary value problem (6.6) are unknown in Ω , since f_1 is unknown. However, the data $\langle \mathbf{g}^0, \mathbf{g}^1 \rangle$ in (6.6d) are known on Γ from Doppler data $\langle I^0\mathbf{f}, I^1\mathbf{f} \rangle$ via (6.3).

6.1. Reconstruction. Given the Doppler data $\langle I^0\mathbf{f}, I^1\mathbf{f} \rangle$, we recover f_1 in (6.4e) and thus \mathbf{f} as follows:

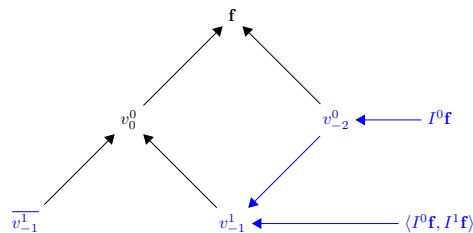


FIGURE 2. Flow of the reconstruction of the vector field \mathbf{f} . In the sweep down, the modes v_{-2}^0 and v_{-1}^1 colored in blue are determined layer by layer from the momenta Doppler data $\langle I^0\mathbf{f}, I^1\mathbf{f} \rangle$ and the previous layer. In the sweep up, also layer by layer starting from the bottom, the remaining coefficient v_0^0 is recovered.

- **Step 1 (Sweep down): The recovery of the sequence $L\mathbf{v}^0$.**

From (6.6b), we note that $L\mathbf{v}^0$ is L^2 -analytic, and can be recovered via the Bukhgeim-Cauchy Integral formula (B.3):

$$(6.7) \quad L\mathbf{v}^0 = \mathcal{B}(L\mathbf{g}^0).$$

Componentwise, for $n \geq 1$,

$$(6.8) \quad v_{-n}^0(z) = \frac{1}{2\pi_1} \int_{\Gamma} \frac{g_{-n}^0(\zeta)}{\zeta - z} d\zeta + \frac{1}{2\pi_1} \int_{\Gamma} \left\{ \frac{d\zeta}{\zeta - z} - \frac{d\bar{\zeta}}{\bar{\zeta} - \bar{z}} \right\} \sum_{j=1}^{\infty} g_{-n-2j}^0(\zeta) \left(\frac{\bar{\zeta} - \bar{z}}{\zeta - z} \right)^j, \quad z \in \Omega.$$

Note that the mode v_0^0 is not yet determined.

- **Step 2 (Sweep down): The recovery of the entire sequence \mathbf{v}^1 .**

Since the modes $\langle v_{-1}^0, v_{-2}^0, v_{-3}^0, \dots \rangle$ are now recovered in Ω by (6.8), the right hand side of the non-homogeneous Bukhgeim Beltrami system (6.6c) is known. The solution \mathbf{v}^1 of (6.6c) and (6.6d) is given by the Bukhgeim-Pompeiu formula (B.6):

$$(6.9) \quad \mathbf{v}^1 = \mathcal{B}\mathbf{g}^1 + \mathcal{T}(L\mathbf{v}^0) = \mathcal{B}\mathbf{g}^1 + \mathcal{T}[\mathcal{B}L\mathbf{g}^0]$$

where the last equality uses (6.7).

While the entire sequence \mathbf{v}^1 is determined, we only need the v_{-1}^1 component:

$$(6.10) \quad \begin{aligned} v_{-1}^1(z) := & \frac{1}{2\pi_1} \int_{\Gamma} \frac{g_{-1}^1(\zeta)}{\zeta - z} d\zeta + \frac{1}{2\pi_1} \int_{\Gamma} \left\{ \frac{d\zeta}{\zeta - z} - \frac{d\bar{\zeta}}{\bar{\zeta} - \bar{z}} \right\} \sum_{j=1}^{\infty} g_{-1-2j}^1(\zeta) \left(\frac{\bar{\zeta} - \bar{z}}{\zeta - z} \right)^j \\ & - \frac{1}{\pi} \sum_{j=0}^{\infty} \int_{\Omega} \frac{v_{-2-2j}^0(\zeta)}{\zeta - z} \left(\frac{\bar{\zeta} - \bar{z}}{\zeta - z} \right)^j d\xi d\eta, \quad \zeta = \xi + i\eta, \quad z \in \Omega. \end{aligned}$$

- **Step 3 (Sweep up): The reconstruction of the Fourier mode v_0^0 .**

The real valued Fourier mode v_0^0 is determined via equation (6.4c) for $n = 1$, and complex conjugate relation (6.5), by

$$(6.11) \quad v_0^0(z) := \bar{\partial}v_1^1(z) + \partial v_{-1}^1(z) = 2 \operatorname{Re} \partial v_{-1}^1(z), \quad z \in \Omega.$$

Thus, from (6.8) and (6.11), the entire sequence $\mathbf{v}^0 = \langle v_0^0, v_{-1}^0, \dots \rangle$ is now determined in Ω .

- **Step 4: The recovery of the vector field \mathbf{f} .**

From the mode v_{-2}^0 in (6.8) for $n = 2$, and the mode v_0^0 in (6.11), we use (6.6a) to recover

$$(6.12) \quad f_1(z) := \bar{\partial}v_0^0(z) + \partial v_{-2}^0(z), \quad z \in \Omega,$$

and define the vector field inside Ω by

$$(6.13) \quad \mathbf{f} := \langle 2 \operatorname{Re} f_1, 2 \operatorname{Im} f_1 \rangle.$$

6.2. Numerical Implementation. We present the results of the reconstruction in three numerical examples. To emphasize the departure from existing works recovering the solenoidal part, in the first two examples the Doppler data is simulated for two different vector fields sharing the same solenoidal part. The third example considers a rough field, with an embedded inclusion. The reconstruction from both noiseless and noisy data is performed for each example. The domain Ω is the unit disk centered at the origin and its boundary Γ is the unit circle.

Starting from a vector field \mathbf{f} , the data is computed by numerical integration in (6.1) and (6.2) via the composite mid-point rule along lines. The data is calculated at 1,440 boundary points $x \in \Gamma$ of equal angular spacing, and at about 720 equiangular outgoing directions $\boldsymbol{\theta} \in \mathbb{S}^1$ (satisfying $x \cdot \boldsymbol{\theta} > 0$).

To avoid an inverse crime, the reconstruction algorithm uses a different numerical path: each component of the vector field is recovered as a piecewise constant approximation on a (1,750 elements) triangular partition of Ω . We use (6.8) to compute the values of v_{-n}^0 at the vertices of the partition, yielding a piecewise linear approximation to v_{-n}^0 . More precisely, if $v_{-n}^0 \approx ax_1 + bx_2 + c$ on a triangle τ , then $\partial v_{-n}^0|_{\tau} \approx \frac{1}{2}(a - b)$ as a piecewise constant approximation required in (6.12). In contrast, the mode v_{-1}^1 is computed at each centroid by (6.10). More precisely, at the centroid c of each triangle τ ,

$$\begin{aligned} v_{-1}^1(c + \lambda) &\approx v_{-1}^1(c) + \partial_{x_1} v_{-1}^1(c)\lambda_1 + \partial_{x_2} v_{-1}^1(c)\lambda_2 \\ &\quad + \frac{1}{2}\partial_{x_1 x_1}^2 v_{-1}^1(c)\lambda_1^2 + \partial_{x_1 x_2}^2 v_{-1}^1(c)\lambda_1\lambda_2 + \frac{1}{2}\partial_{x_2 x_2}^2 v_{-1}^1(c)\lambda_2^2 \end{aligned}$$

for small $\lambda = (\lambda_1, \lambda_2)$. We write $\tau_1, \tau_2, \dots, \tau_K$ the triangles sharing vertices or edges with τ . Then substituting $\lambda = c - c_k, k = 1, 2, \dots, K$ to the expansion, we obtain K linear constraints with five unknowns $\partial_{x_1} v_{-1}^1(c), \partial_{x_2} v_{-1}^1(c), \partial_{x_1 x_1}^2 v_{-1}^1(c), \partial_{x_1 x_2}^2 v_{-1}^1(c),$ and $\partial_{x_2 x_2}^2 v_{-1}^1(c)$ required in (6.12) with (6.11) to find \bar{v}_0^0 . The least square method leads a unique solution to them on each τ . The boundary integrals in (6.8) and (6.10) are approximated by the composite mid-point rule as the sum of the product of mid-point values of the integrand and arc lengths [16]. Note that the singularity of the integrand of the final term in (6.10) is removable and a conventional mid-point numerical integration rule can be applied. More precisely, we use

$$\begin{aligned} \int_{\Omega} \frac{v_{-2-2j}^0(\zeta)}{\zeta - z} \left(\frac{\bar{\zeta} - \bar{z}}{\zeta - z} \right)^j d\xi d\eta &\approx \sum_m v_{-2-2j}^0(c_m) \int_{\tau_m} \frac{1}{\zeta - z} \left(\frac{\bar{\zeta} - \bar{z}}{\zeta - z} \right)^j d\xi d\eta \\ &= \sum_m v_{-2-2j}^0(c_m) \int_{-\pi}^{\pi} \rho_m(z; \varphi) e^{-(2j+1)i\varphi} d\varphi, \end{aligned}$$

where $\{\tau_m\}$ gives a triangulation of Ω , c_m is the centroid of τ_m , and $\rho_m(z; \varphi)$ is the length of the half-line starting from z in the φ -direction cut by the triangle τ_m ; if z belongs to τ_m , then τ_m is the distance between z and $\partial\tau_m$ in the φ -direction (Fig. 3). The last integral above is computed by the eight-point Gauss-Legendre rule with algebraically calculated ρ_m as explained in the figure below.



FIGURE 3. The length $\rho_m(z; \varphi)$ cut by the triangle τ_m . The case for $z \notin \tau_m$ (left) and that for $z \in \tau_m$ (right)

Throughout this section, the series in (6.8) and (6.10) are truncated up to 256 Fourier modes. The truncation index not only controls the accuracy, but also plays a regularizing role in stability.

In the examples below, the relative error between a reconstructed vector field $\mathbf{f}_{\text{recon}}$ and the exact one are in the L^2 sense:

$$(6.14) \quad \|\mathbf{f}_{\text{recon}} - \mathbf{f}\|_{\text{rel}} = \frac{\|\mathbf{f}_{\text{recon}} - \mathbf{f}\|_2}{\|\mathbf{f}\|_2}.$$

Similarly, the relative error in the data is in the L^2 sense.

All numerically reconstructed results are calculated in the double precision arithmetic on AMD EPYC 7643 with 96 threads OpenMP parallel computations.

Example 1. We consider first the vector field

$$(6.15) \quad \mathbf{f}(x) = \nabla (\sin \pi |x|^2) + \mathbf{f}^s(x),$$

where the solenoidal part

$$(6.16) \quad \mathbf{f}^s(x) = \begin{pmatrix} 2x_1x_2 \cos |x|^2 + \cos(6x_1x_2) - 6x_1x_2 \sin(6x_1x_2) \\ -\sin |x|^2 - 2x_1^2 \cos |x|^2 + 6x_2^2 \sin(6x_1x_2) \end{pmatrix};$$

see [20] and Figure 5 below.

Example 1(a) - Noiseless data: For the vector field \mathbf{f} in (6.15), the simulated data ($I^0\mathbf{f}, I^1\mathbf{f}$) is illustrated in Figure 4, where crosses (\times) depict a few boundary nodes $x \in \Gamma$, while the red and blue curves are $\{x + |I^j\mathbf{f}(x, \boldsymbol{\theta})|\boldsymbol{\theta}; \boldsymbol{\theta} \in \mathbb{S}^1, x \cdot \boldsymbol{\theta} > 0\}$, $j = 0, 1$. Also, for illustration purposes, the radial direction is shrunk by $1/5$ -th.

Note that $I^0\mathbf{f}$, and $I^1\mathbf{f}$, are not always positive. To differentiate the sign, the positive and negative parts are drawn in red, respectively in blue. Since only outgoing signals are measured (while the incoming flow is zero at the boundary) signals are depicted outside Ω only.

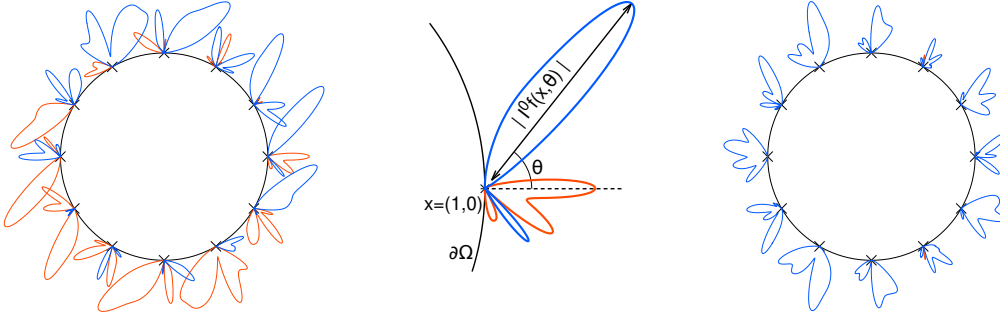


FIGURE 4. Simulated data for \mathbf{f} in (6.15): $I^0\mathbf{f}$ (left) with its magnification at $x = (1, 0)$ (middle), and $I^1\mathbf{f}$ (right). The crosses (\times) are some data collection points at the boundary, while the red and blue curves represent $I^j\mathbf{f}(x, \boldsymbol{\theta})$, $j = 0, 1$ in polar coordinates $(|I^j\mathbf{f}(x, \boldsymbol{\theta})|, \boldsymbol{\theta})$ centered at the respective boundary point $x \in \Gamma$. The radial direction is shrunk by $1/5$ -th for illustration purposes.

The numerically reconstructed result shown in Figure 6 has a relative error of 18.1%. The total elapsed time in the reconstruction is approximately 10 seconds.

Example 1(b) - Perturbed data within the range: To illustrate the stability estimate in Theorem 2.1, we first consider the case of data perturbed within the range. To generate such a data we solve the forward problem by (6.1) and (6.2) for a perturbed vector field $\mathbf{f}_\epsilon = \mathbf{f} + \epsilon$, for some smooth vector field ϵ in Ω . Figure 7 below shows the reconstruction $\mathbf{f}_{\epsilon, \text{recon}}$ from this data. In this example, the relative error in the data for $I^0\mathbf{f}$ is 5.52% and for $I^1\mathbf{f}$ is 4.48%, while the relative error in the reconstruction is 30.0%.

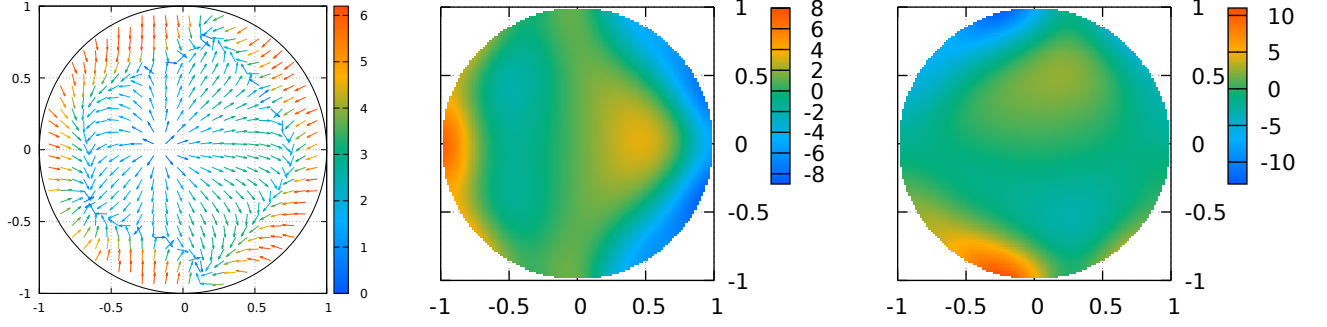


FIGURE 5. Exact vector field $\mathbf{f} = \langle F_1, F_2 \rangle$ in (6.15) (left), its first component F_1 (middle) and its second component F_2 (right).

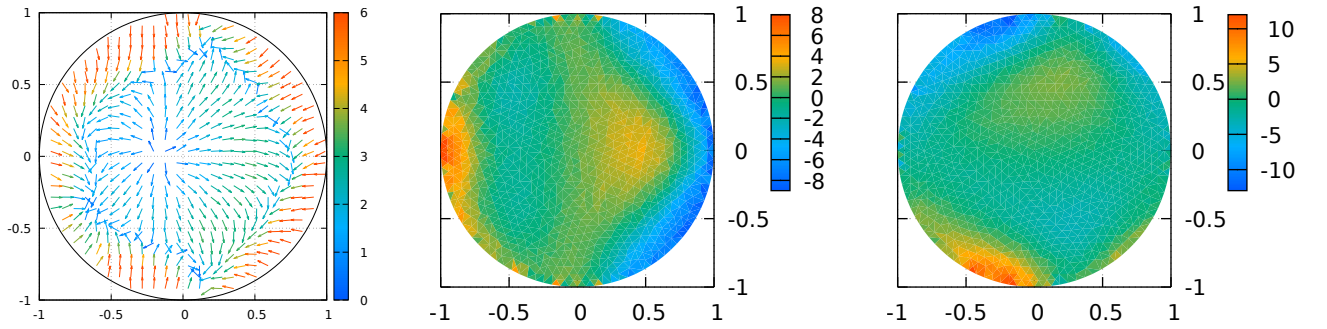


FIGURE 6. Numerical reconstruction from noiseless data: The vector field $\mathbf{f}_{0,\text{recon}}$ (left), its first component F_1 (middle) and its second component F_2 (right).

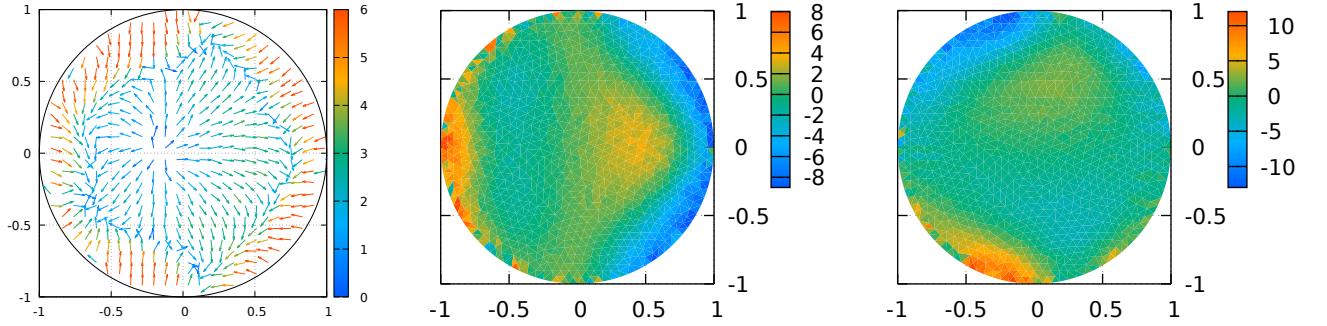


FIGURE 7. Numerical reconstruction from perturbed data within the range (5.52% relative error in $I^0\mathbf{f}$ and 4.48% in $I^1\mathbf{f}$). The reconstructed field $\mathbf{f}_{\epsilon,\text{recon}} = \langle F_1, F_2 \rangle$ (left) and its components F_1 (middle) and F_2 (right) has 30.0% relative error.

Example 1(c) - Noisy data : To assess the robustness of the method, we consider the same vector field as in (6.15), where the data is corrupted with an additive random error. Specifically, $I^0\mathbf{f}$ now contains about 5.88% relative error, while $I^1\mathbf{f}$ contains 4.34% relative error, which are at the same level as in the previous example; see Figure 8 for an illustration.

The reconstructed vector field $\mathbf{f}_{\text{recon}}$ shown in Figure 9, contains approximately 54.6% relative error.

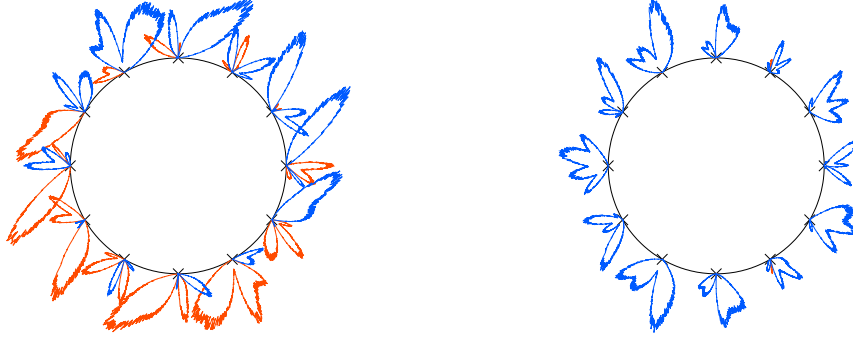


FIGURE 8. Noisy data $I^0\mathbf{f}$ (left) with 5.88% error and $I^1\mathbf{f}$ (right) with 4.34% error.

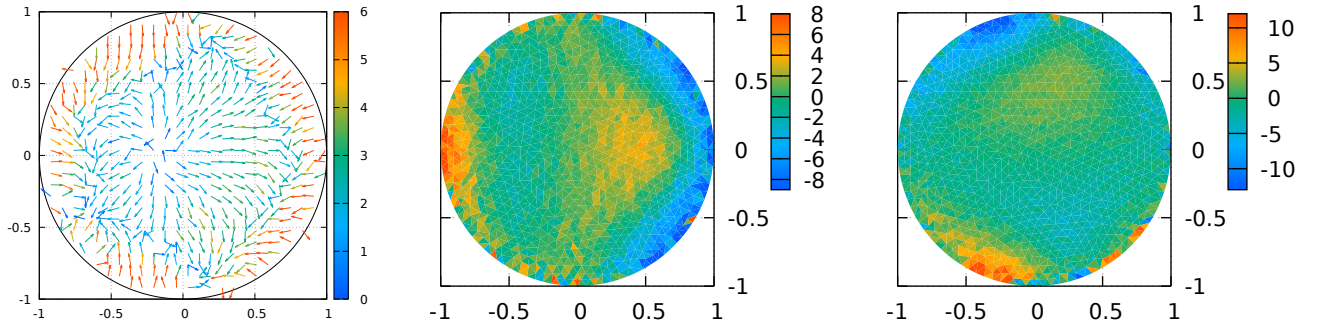


FIGURE 9. Numerical reconstruction from noisy data (5.88% relative error in $I^0\mathbf{f}$ and 4.34% in $I^1\mathbf{f}$). The reconstructed field $\mathbf{f}_{\text{recon}} = \langle F_1, F_2 \rangle$ (left) and its components F_1 (middle) and F_2 (right) has 54.6% relative error.

Example 2. We consider next the vector field

$$(6.17) \quad \mathbf{f}(x) = \nabla \left(\arctan \frac{x_2}{2 + x_1} \right) + \mathbf{f}^s(x)$$

with the same solenoidal part \mathbf{f}^s as in (6.16).

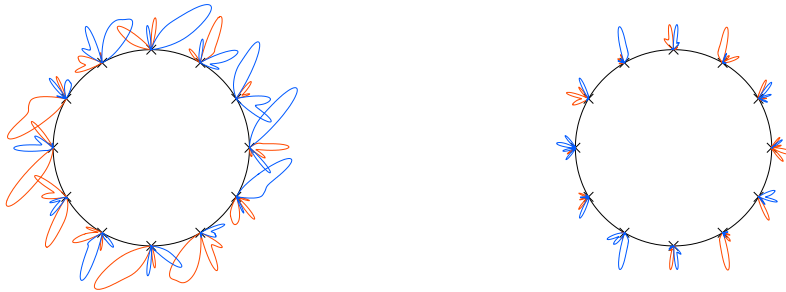


FIGURE 10. Simulated noiseless data $I^0\mathbf{f}$ (left) and $I^1\mathbf{f}$ (right) for \mathbf{f} in (6.17). The crosses (\times) are some data collection points at the boundary, while the red and blue curves represent $I^j\mathbf{f}(x, \boldsymbol{\theta})$, $j = 0, 1$ in polar coordinates $(|I^j\mathbf{f}(x, \boldsymbol{\theta})|, \boldsymbol{\theta})$ centered at the respective boundary point $x \in \Gamma$.

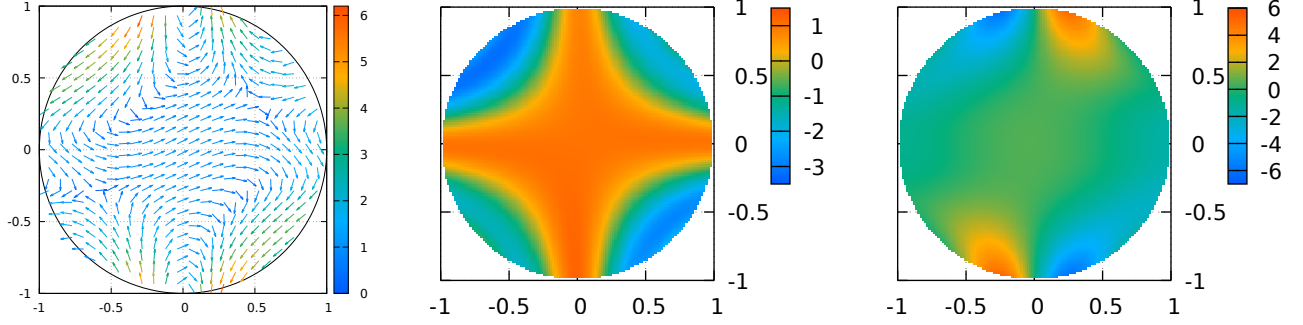


FIGURE 11. Exact vector field $\mathbf{f} = \langle F_1, F_2 \rangle$ in (6.17) (left), its first component F_1 (middle) and its second component F_2 (right).

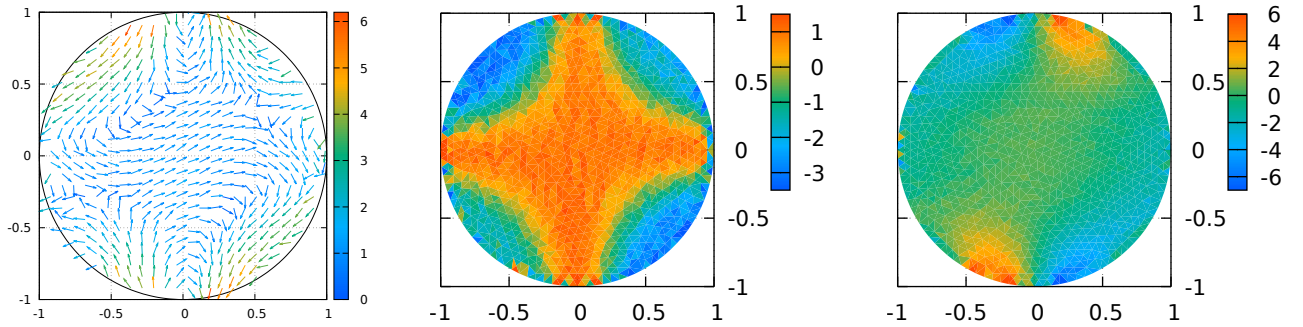


FIGURE 12. Numerically reconstructed vector field from noiseless Doppler data: vector field $\mathbf{f}_{0,\text{recon}} = \langle F_1, F_2 \rangle$ (left) and its components F_1 (middle) and F_2 (right).

Example 2(a) - Noiseless data: The vector field in (6.17) is depicted in Figure 11, while its corresponding simulated Doppler data is shown in Figure 10. The numerically reconstructed vector field and its components are exhibited in Figure 12 having 31.1% relative error.

Example 2(b) - Perturbed data within the range: In this case, the generated perturbed data \mathbf{f}_ϵ depicted in Figure 13 has 5.02% relative error in $I^0\mathbf{f}$ and 6.04% relative error in $I^1\mathbf{f}$. The numerical reconstruction of $\mathbf{f}_{\epsilon,\text{recon}}$ in Figure 14 has 45.9% relative error.

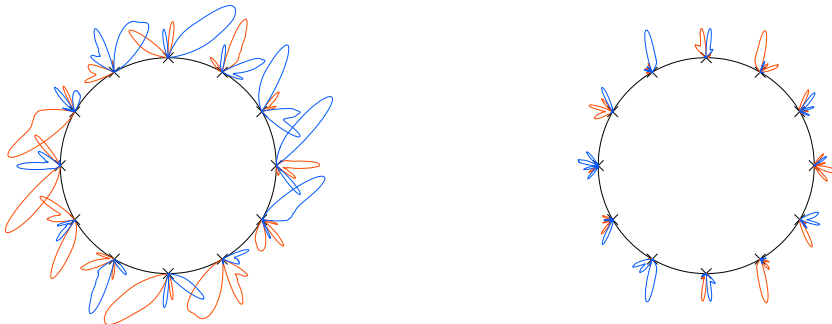


FIGURE 13. Data $I^0\mathbf{f}_\epsilon$ (left) with 5.02% error and $I^1\mathbf{f}_\epsilon$ (right) with 6.04% error, which is considered as measurement data with noise in range

Example 2(c) - Noisy data: We consider the same vector field as in (6.17), however the data is corrupted with additive random errors: 6.03% relative error in $I^0\mathbf{f}$, and 5.04% in $I^1\mathbf{f}$.

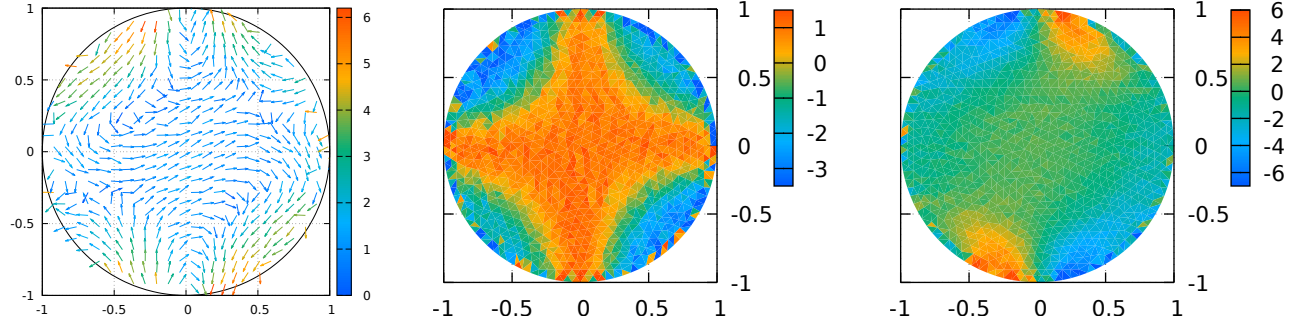


FIGURE 14. Numerical reconstruction from perturbed data within the range (5.02% relative error in $I^0\mathbf{f}$ and 6.04% in $I^1\mathbf{f}$). The reconstructed field $\mathbf{f}_{e,\text{recon}} = \langle F_1, F_2 \rangle$ (left) and its components F_1 (middle) and F_2 (right) has 45.9% relative error.

The numerical reconstruction results are shown in Figure 15. The reconstructed vector field $\mathbf{f}_{\text{recon}}$ has 71.3% relative error.

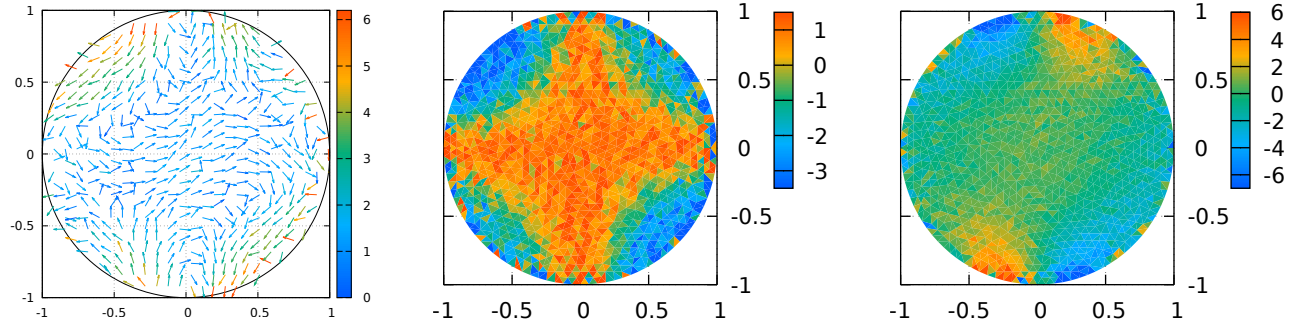


FIGURE 15. Numerical reconstruction from noisy data (6.03% relative error in $I^0\mathbf{f}$ and 5.04% in $I^1\mathbf{f}$). The reconstructed field $\mathbf{f}_{\text{recon}} = \langle F_1, F_2 \rangle$ (left) and its components F_1 (middle) and F_2 (right) has 71.3% relative error.

In Table 1 below, we summarize the level of error obtained in the examples. The reconstruction error in Example 1(b) (30.0%), respectively, Example 2(b) (45.9%) obtained from the perturbed data within the range reflects the instability of our method due to twice differentiation. The reconstruction error in Example 1(c) (54.6%), respectively, Example 2(c) (71.3%) obtained from (an additive random error) noisy data is also due to the ill-posedness (non-existence) specific to inverting data outside the range.

TABLE 1. Differences between noiseless data, perturbed data in the range and additive random noise in the first two examples.

Relative error in	Ex 1 (a)	Ex 1 (b)	Ex 1 (c)	Ex 2 (a)	Ex 2 (b)	Ex 2 (c)
$I^0\mathbf{f}$	0%	5.52%	5.88%	0%	5.02%	6.03%
$I^1\mathbf{f}$	0%	4.48%	4.34%	0%	6.04%	5.04%
Reconstruction	18.1%	30.0%	54.6%	31.1%	45.9%	71.3%

Example 3. Let $S = [-0.25, 0.75] \times [-0.5, 0.5]$ be an off-centered square and denote by χ_S its characteristic function. Then we consider a vector field supported by S :

$$(6.18) \quad \mathbf{f}(x) = \chi_S(x) \begin{pmatrix} (1 - (2x_1 - 0.5)^2)(1 - 4x_2^2) \\ \cos((2x_1 + 0.5)\pi) \cos(2\pi x_2) \end{pmatrix}.$$

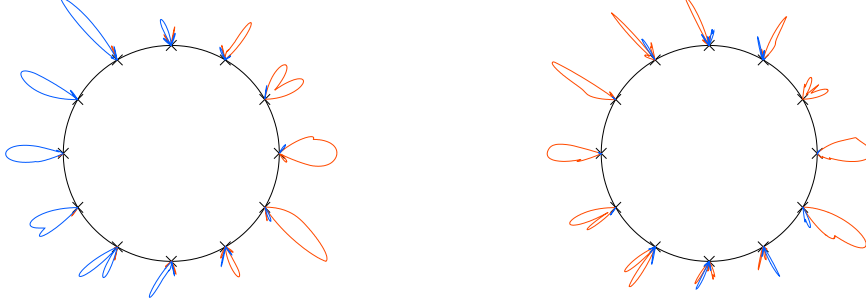


FIGURE 16. Simulated noiseless data $I^0 \mathbf{f}$ (left) and $I^1 \mathbf{f}$ (right) for \mathbf{f} in (6.18). The crosses (\times) are some data collection points at the boundary, while the red and blue curves represent $I^j \mathbf{f}(x, \boldsymbol{\theta})$, $j = 0, 1$ in polar coordinates $(|I^j \mathbf{f}(x, \boldsymbol{\theta})|, \boldsymbol{\theta})$ centered at the respective boundary point $x \in \Gamma$.

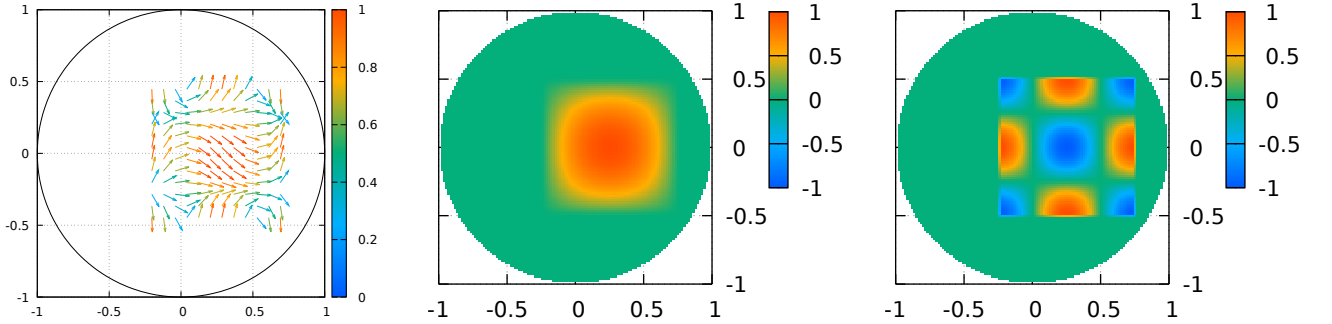


FIGURE 17. Exact vector field \mathbf{f} in (6.18) (left), its first component F_1 (middle) and its second component F_2 (right).

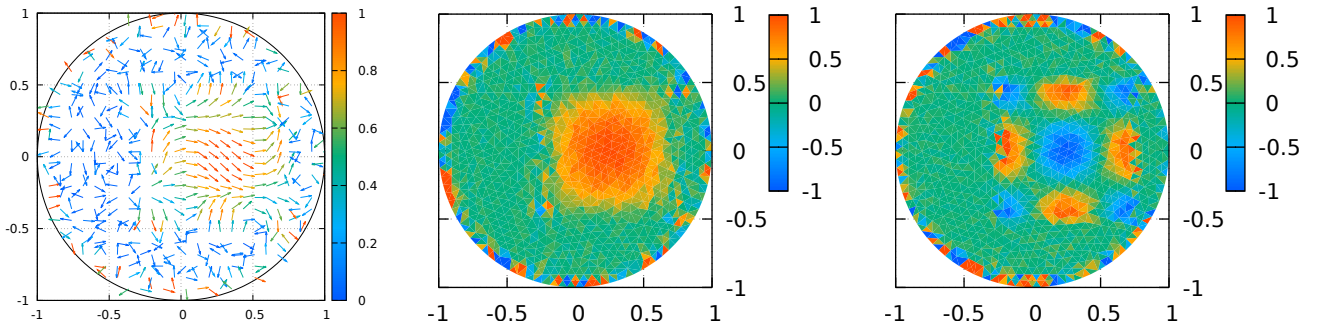


FIGURE 18. Numerically reconstructed vector field from noiseless Doppler data: vector field $\mathbf{f}_{0,\text{recon}} = \langle F_1, F_2 \rangle$ (left) and its components F_1 (middle) and F_2 (right).

TABLE 2. Errors measured in subdomains of Ω for Example 3

	(a) Noiseless case	(b) Random Noise case
$L^2(\Omega)$	125.5%	141.9%
Number of triangles	1,750	
$L^2(x < 0.95)$	52.5%	61.2%
Number of triangles	1,552	

Example 3(a) - Noiseless data: The vector field in (6.18) is given in Figure 17, while its corresponding simulated Doppler data is shown in Figure 16. The numerically reconstructed vector field and its components are exhibited in Figure 18.

Example 3(b) - Noisy data: We consider the same vector field as in (6.18), however the data is corrupted with additive random errors: 5.52% relative error in $I^0\mathbf{f}$, and 4.61% in $I^1\mathbf{f}$. The numerical reconstruction results are shown in Figure 19. Even though \mathbf{f} has discontinuity along ∂S , the support of \mathbf{f} can be clearly distinguished.

Fig. 18 and Fig. 19 indicate that the large error appear near the boundary. Table 2 shows this fact quantitatively. In the whole domain, the relative L^2 error of reconstructed vector fields from noiseless data and noisy data are 125.5% and 141.9% respectively. If we measure the errors in triangles whose centers $c = (c_1, c_2)$ locate in $|c| < 0.95$, errors are 52.5% and 61.2% respectively. The number of triangles are 1,552 which is 88.7% of total number of triangles (1,750) in Ω , while the errors are less than half.

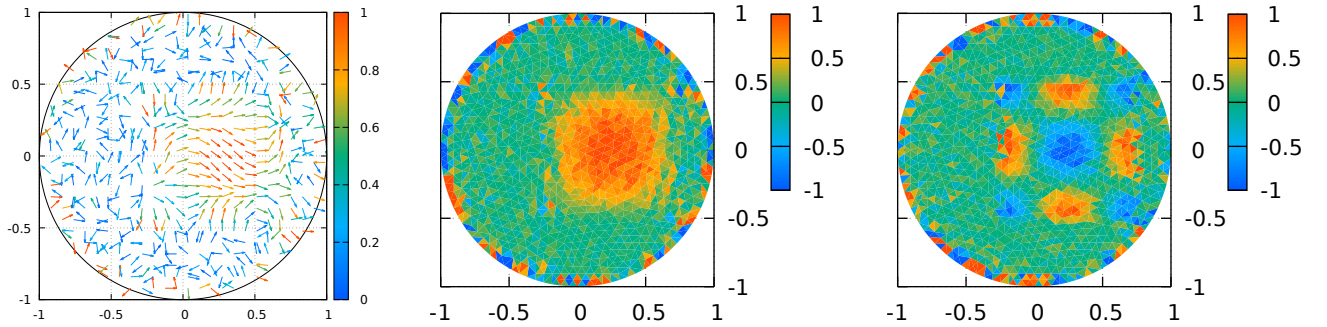


FIGURE 19. Numerical reconstruction from noisy data (5.52% relative error in $I^0\mathbf{f}$ and 4.61% in $I^1\mathbf{f}$).

7. CONCLUSION

We reduced the inversion of the non/attenuated momenta-ray transform of symmetric real valued m -tensors to an inverse boundary value problem for a weakly coupled system of transport equations. In the plane, the latter is solved by an extension of Bukhgeim's theory of A -analytic maps. The inversion method does not require the Helmholtz decomposition and applies to sufficiently smooth planar tensors of arbitrary order. The stability estimates obtained here show that our reconstruction method is as ill-posed as taking $m + 1^{st}$ derivatives, where m is the order of the tensor fields. For the Doppler ($m = 1$) case, the method is feasible as showcased here in results obtained in its numerical implementation. For higher order tensors the reconstruction would require either some additional regularization, or transversal information.

ACKNOWLEDGMENT

The work of H. Fujiwara was supported by JSPS KAKENHI Grant Numbers JP20H01821, JP21H00999 and JP22K18674. The work of A. Tamasan was supported in part by the National Science Foundation DMS-1907097. The work of D. Omogbhe was supported in part by the Austrian Science Fund (FWF), Project 10.55776/P31053 and by FWF SFB 10.55776/F68 ‘‘Tomography Across the Scales’’ project F6801-N36. The work of K. Sadiq was supported in part by the FWF Project 10.55776/P31053. For open access purposes, the author has applied a CC BY public copyright license to any author-accepted manuscript version arising from this submission.

APPENDIX A. PROOF OF PROPOSITION 2.1

From (2.2a) and (2.2b), we note that for $(x, \boldsymbol{\theta}) \in \Omega \times \mathbb{S}^1$ and $1 \leq k \leq m$,

$$(A.1) \quad \frac{d}{dt} \left[e^{-\int_t^\infty a(x+s\boldsymbol{\theta})ds} u^0(x+t\boldsymbol{\theta}, \boldsymbol{\theta}) \right] = e^{-\int_t^\infty a(x+s\boldsymbol{\theta})ds} \langle \mathbf{f}(x+t\boldsymbol{\theta}), \boldsymbol{\theta}^m \rangle,$$

$$(A.2) \quad \frac{d}{dt} \left[e^{-\int_t^\infty a(x+s\boldsymbol{\theta})ds} u^k(x+t\boldsymbol{\theta}, \boldsymbol{\theta}) \right] = e^{-\int_t^\infty a(x+s\boldsymbol{\theta})ds} u^{k-1}(x+t\boldsymbol{\theta}, \boldsymbol{\theta}).$$

For $(x, \boldsymbol{\theta}) \in \Omega \times \mathbb{S}^1$ an integration along the line through x in the direction of $\boldsymbol{\theta}$ in (2.2a) together with the zero incoming condition (2.2c) yield

$$(A.3) \quad \begin{aligned} e^{-\int_{x \cdot \boldsymbol{\theta}}^\infty a(\Pi_{\boldsymbol{\theta}}(x)+s\boldsymbol{\theta})ds} u^0(x, \boldsymbol{\theta}) &= \int_{-\infty}^{x \cdot \boldsymbol{\theta}} \frac{d}{dt} \left[e^{-\int_t^\infty a(\Pi_{\boldsymbol{\theta}}(x)+s\boldsymbol{\theta})ds} u^0(\Pi_{\boldsymbol{\theta}}(x) + t\boldsymbol{\theta}, \boldsymbol{\theta}) \right] dt \\ &= \int_{-\infty}^{x \cdot \boldsymbol{\theta}} e^{-\int_t^\infty a(\Pi_{\boldsymbol{\theta}}(x)+s\boldsymbol{\theta})ds} \langle \mathbf{f}(\Pi_{\boldsymbol{\theta}}(x) + t\boldsymbol{\theta}), \boldsymbol{\theta}^m \rangle dt. \end{aligned}$$

Note that $\int_{x \cdot \boldsymbol{\theta}}^\infty a(\Pi_{\boldsymbol{\theta}}(x) + s\boldsymbol{\theta})ds = \int_0^\infty a(x + s\boldsymbol{\theta})ds$.

Similarly, for each $1 \leq k \leq m$ a recursive integration by parts in (2.2b) together with (2.2c) yield

$$\begin{aligned} e^{-\int_{x \cdot \boldsymbol{\theta}}^\infty a(\Pi_{\boldsymbol{\theta}}(x)+s\boldsymbol{\theta})ds} u^k(x, \boldsymbol{\theta}) &= \int_{-\infty}^{x \cdot \boldsymbol{\theta}} \frac{d}{dt} \left[e^{-\int_t^\infty a(\Pi_{\boldsymbol{\theta}}(x)+s\boldsymbol{\theta})ds} u^k(\Pi_{\boldsymbol{\theta}}(x) + t\boldsymbol{\theta}, \boldsymbol{\theta}) \right] dt \\ &= \int_{-\infty}^{x \cdot \boldsymbol{\theta}} e^{-\int_t^\infty a(\Pi_{\boldsymbol{\theta}}(x)+s\boldsymbol{\theta})ds} u^{k-1}(\Pi_{\boldsymbol{\theta}}(x) + t\boldsymbol{\theta}, \boldsymbol{\theta}) dt \\ &= e^{-\int_{x \cdot \boldsymbol{\theta}}^\infty a(\Pi_{\boldsymbol{\theta}}(x)+s\boldsymbol{\theta})ds} \sum_{n=1}^k (-1)^{n-1} \frac{(x \cdot \boldsymbol{\theta})^n}{n!} u^{k-n}(x, \boldsymbol{\theta}) \\ &\quad + (-1)^k \int_{-\infty}^{x \cdot \boldsymbol{\theta}} \frac{t^k}{k!} e^{-\int_t^\infty a(\Pi_{\boldsymbol{\theta}}(x)+s\boldsymbol{\theta})ds} \langle \mathbf{f}(\Pi_{\boldsymbol{\theta}}(x) + t\boldsymbol{\theta}), \boldsymbol{\theta}^m \rangle dt, \end{aligned}$$

where in the last equality we use (A.3). Thus, multiplying both sides of the above equation with $e^{\int_{x \cdot \boldsymbol{\theta}}^\infty a(\Pi_{\boldsymbol{\theta}}(x)+s\boldsymbol{\theta})ds}$ yields

$$(A.4) \quad u^k(x, \boldsymbol{\theta}) = \sum_{n=1}^k (-1)^{n-1} \frac{(x \cdot \boldsymbol{\theta})^n}{n!} u^{k-n}(x, \boldsymbol{\theta}) + (-1)^k \int_{-\infty}^{x \cdot \boldsymbol{\theta}} \frac{t^k}{k!} e^{-\int_t^\infty a(\Pi_{\boldsymbol{\theta}}(x)+s\boldsymbol{\theta})ds} \langle \mathbf{f}(\Pi_{\boldsymbol{\theta}}(x) + t\boldsymbol{\theta}), \boldsymbol{\theta}^m \rangle dt,$$

Since $\mathbf{f}(x + (t - x \cdot \boldsymbol{\theta})\boldsymbol{\theta}) = \mathbf{0}$ for every $(x, \boldsymbol{\theta}) \in \Gamma_+$ and $t > x \cdot \boldsymbol{\theta}$,

$$(A.5) \quad \int_{-\infty}^{x \cdot \boldsymbol{\theta}} t^k e^{-\int_t^{x \cdot \boldsymbol{\theta}} a(\Pi_{\boldsymbol{\theta}}(x) + s\boldsymbol{\theta}) ds} \langle \mathbf{f}(\Pi_{\boldsymbol{\theta}}(x) + t\boldsymbol{\theta}), \boldsymbol{\theta}^m \rangle dt = \int_{-\infty}^{\infty} t^k e^{-\int_t^{x \cdot \boldsymbol{\theta}} a(\Pi_{\boldsymbol{\theta}}(x) + s\boldsymbol{\theta}) ds} \langle \mathbf{f}(\Pi_{\boldsymbol{\theta}}(x) + t\boldsymbol{\theta}), \boldsymbol{\theta}^m \rangle dt = I_a^k \mathbf{f}(x, \boldsymbol{\theta}).$$

The relations (2.3) now follow from (A.4), (A.3), and (A.5).

Since $\mathbf{f} \in H_0^s(\mathbf{S}^m; \Omega)$, $s \geq 1$ and $a \in C^{s, \mu}(\bar{\Omega})$, $\mu > 1/2$, the solution u^0 given by (A.3) preserves the regularity and $u^0 \in H^s(\Omega \times \mathbb{S}^1)$. Moreover, by (2.2b) and (A.4), $u^k \in H^s(\Omega \times \mathbb{S}^1)$, $s \geq 1$ for $1 \leq k \leq m$. \square

APPENDIX B. AN EXPLICIT POMPEIU FORMULA FOR L^2 -ANALYTIC MAPS

In this section we derive a Pompeiu type formula corresponding to A -analytic maps. The domain Ω is strictly convex but need not be a disc.

Bukhgeim's original theory in [8] shows that solutions (called L^2 -analytic) of the homogenous Beltrami-like equation

$$(B.1) \quad \bar{\partial} \mathbf{v}(z) + L^2 \partial \mathbf{v}(z) = \mathbf{0}, \quad z \in \Omega,$$

satisfy a Cauchy-like integral formula,

$$(B.2) \quad \mathbf{v}(z) = \mathcal{B}[\mathbf{v}|_{\Gamma}](z), \quad z \in \Omega,$$

where \mathcal{B} is defined component-wise for $n \geq 0$ by

$$(B.3) \quad (\mathcal{B}\mathbf{v})_{-n}(z) := \frac{1}{2\pi i} \int_{\Gamma} \frac{v_{-n}(\zeta)}{\zeta - z} d\zeta + \frac{1}{2\pi i} \int_{\Gamma} \left\{ \frac{d\zeta}{\zeta - z} - \frac{d\bar{\zeta}}{\bar{\zeta} - \bar{z}} \right\} \sum_{j=1}^{\infty} v_{-n-2j}(\zeta) \left(\frac{\bar{\zeta} - \bar{z}}{\zeta - z} \right)^j, \quad z \in \Omega.$$

For the inhomogeneous Bukhgeim-Beltrami equation

$$(B.4) \quad \bar{\partial} \mathbf{v} + L^2 \partial \mathbf{v} = \mathbf{w},$$

we introduce here a Pompeiu like operator \mathcal{T} defined component-wise for $n \geq 0$ by

$$(B.5) \quad (\mathcal{T}\mathbf{w})_{-n}(z) := -\frac{1}{\pi} \sum_{j=0}^{\infty} \int_{\Omega} w_{-n-2j}(\zeta) \frac{1}{\zeta - z} \left(\frac{\bar{\zeta} - \bar{z}}{\zeta - z} \right)^j d\xi d\eta, \quad \zeta = \xi + i\eta, \quad z \in \Omega.$$

Proposition B.1. *Let Ω be bounded convex domain with C^1 boundary, \mathcal{B} and \mathcal{T} be the operators in (B.3), respectively, (B.5), and $\mathbf{w} \in C(\bar{\Omega}; l^1)$. If $\mathbf{v} \in C^1(\Omega; l^1) \cap C(\bar{\Omega}; l^1)$ solves (B.4), then*

$$(B.6) \quad \mathbf{v}(z) = \mathcal{B}[\mathbf{v}|_{\Gamma}](z) + (\mathcal{T}\mathbf{w})(z), \quad z \in \Omega.$$

Proof. For $n \geq 0$, consider

$$(B.7) \quad \sigma_{-n}(z, \varphi) = \sum_{j=0}^{\infty} v_{-n-2j}(z) e^{-i(n+2j)\varphi},$$

as in [14]. It is easy to see that $\sigma_{-n} \in C^1(\Omega) \cap C(\bar{\Omega})$.

Let $z \in \Omega$ be arbitrarily fixed. We parametrize $\bar{\Omega}$ in polar coordinates

$$\zeta(\varphi) = z + te^{i\varphi}, \quad 0 \leq t \leq l(\varphi) := \text{dist}(z, \Gamma), \quad 0 \leq \varphi \leq 2\pi.$$

Then

$$(B.8) \quad e^{-2i\varphi} = \frac{\bar{\zeta} - \bar{z}}{\zeta - z}, \quad d\varphi = \frac{1}{2i} \left(\frac{1}{\zeta - z} d\zeta - \frac{1}{\bar{\zeta} - \bar{z}} d\bar{\zeta} \right).$$

The equation (B.4) written in component-wise form is

$$(B.9) \quad \bar{\partial}v_{-n}(z) + \partial v_{-n-2}(z) = w_{-n}(z), \quad z \in \Omega, \quad n \in \mathbb{Z}.$$

For $n \geq 0$, evaluate for each $\varphi \in [0, 2\pi]$

$$(B.10) \quad \begin{aligned} \sigma_{-n}(\zeta, \varphi) - \sigma_{-n}(z, \varphi) &= \int_0^l \frac{\partial \sigma_{-n}}{\partial t}(z + te^{i\varphi}, \varphi) dt = \int_0^l \left(\frac{\partial \sigma_{-n}}{\partial \bar{z}} e^{-i\varphi} + \frac{\partial \sigma_{-n}}{\partial z} e^{i\varphi} \right) dt \\ &= \int_0^l \frac{\partial v_{-n}}{\partial z} e^{-i(n-1)\varphi} dt + \int_0^l \sum_{j=0}^{\infty} \left(\bar{\partial}v_{-n-2j} + \partial v_{-n-2j-2} \right) e^{-i(n+2j+1)\varphi} dt. \end{aligned}$$

From (B.7), $v_{-n}(z)$ is the n -th Fourier coefficient of $\sigma_{-n}(z, \cdot)$. Thus,

$$(B.11) \quad \begin{aligned} v_{-n}(z) &= \frac{1}{2\pi} \int_0^{2\pi} \sigma_{-n}(z, \varphi) e^{in\varphi} d\varphi \\ &= \frac{1}{2\pi} \int_0^{2\pi} \sigma_{-n}(\zeta, \varphi) e^{in\varphi} d\varphi - \frac{1}{2\pi} \int_0^{2\pi} \int_0^{l(\varphi)} \partial v_{-n} \frac{1}{te^{-i\varphi}} t dt d\varphi \\ &\quad - \frac{1}{2\pi} \int_0^{2\pi} \int_0^{l(\varphi)} \sum_{j=0}^{\infty} \left(\bar{\partial}v_{-n-2j} + \partial v_{-n-2j-2} \right) e^{-2ij\varphi} \frac{1}{te^{i\varphi}} t dt d\varphi \\ &= \frac{1}{2\pi} \int_0^{2\pi} \sum_{j=0}^{\infty} v_{-n-2j}(\zeta) e^{-2ij\varphi} d\varphi - \frac{1}{2\pi} \int_{\Omega} \partial v_{-n} \frac{1}{\zeta - \bar{z}} d\xi d\eta \\ &\quad - \frac{1}{2\pi} \int_{\Omega} \sum_{j=0}^{\infty} \left(\bar{\partial}v_{-n-2j} + \partial v_{-n-2j-2} \right) e^{-2ij\varphi} \frac{1}{\zeta - z} d\xi d\eta, \quad \zeta = \xi + i\eta, \end{aligned}$$

where the second equality uses (B.10).

By the conjugate form of the Cauchy-Pompeiu formula (e.g. see [43]), we have

$$(B.12) \quad \frac{1}{2\pi} \int_{\Omega} \bar{\partial}v_{-n} \frac{1}{\zeta - z} d\xi d\eta = \frac{1}{2} v_{-n}(z) + \frac{1}{4\pi i} \int_{\partial\Omega} v_{-n}(\zeta) \frac{1}{\bar{\zeta} - \bar{z}} d\bar{\zeta}.$$

Substituting (B.9), (B.8), and (B.12) into (B.11) yields

$$(B.13) \quad \begin{aligned} v_{-n}(z) &= \frac{1}{2\pi i} \int_{\Gamma} \frac{v_{-n}(\zeta)}{\zeta - z} d\zeta + \frac{1}{2\pi i} \int_{\Gamma} \left\{ \frac{d\zeta}{\zeta - z} - \frac{d\bar{\zeta}}{\bar{\zeta} - \bar{z}} \right\} \sum_{j=1}^{\infty} v_{-n-2j}(\zeta) \left(\frac{\bar{\zeta} - \bar{z}}{\zeta - z} \right)^j \\ &\quad - \frac{1}{\pi} \sum_{j=0}^{\infty} \int_{\Omega} w_{-n-2j}(\zeta) \frac{1}{\zeta - z} \left(\frac{\bar{\zeta} - \bar{z}}{\zeta - z} \right)^j d\xi d\eta, \quad \zeta = \xi + i\eta. \end{aligned}$$

□

REFERENCES

- [1] B. Abbey, S. Zhang, M. Xie, X. Song, A. Korsunsky, *Neutron strain tomography using bragg-edge transmission*, International journal of materials research **103** (2) (2012), 234–241.
- [2] H. Aben, *Integrated Photoelasticity*, McGraw-Hill, New York, 1979.
- [3] A. Abhishek and R. K. Mishra, *Support theorems and an injectivity result for integral moments of a symmetric m -tensor field*, J. Fourier Anal. Appl., **25** (4) (2019), 1487–1512.
- [4] F. Andersson, *The Doppler moment transform in Doppler tomography*, Inverse Problems **21** (2005), 1249–1274.
- [5] E. V. Arbutov, A. L. Bukhgeim and S. G. Kazantsev, *Two-dimensional tomography problems and the theory of A -analytic functions*, Siberian Adv. Math., **8** (1998), 1–20.
- [6] G. Bal, *On the attenuated Radon transform with full and partial measurements*, Inverse Problems **20** (2004), 399–418.
- [7] H. Braun and A. Hauk, *Tomographic reconstruction of vector fields*, IEEE Transactions on signal processing **39** (1991), 464–471.
- [8] A. L. Bukhgeim, *Inversion Formulas in Inverse Problems*, chapter in Linear Operators and Ill-Posed Problems by M. M. Lavrentiev and L. Ya. Savalev, Plenum, New York, 1995.
- [9] E. Derevtsov, *Ray Transforms of the Moments of Planar Tensor Fields*, J. Appl. Ind. Math., **17** (2023), 521–534.
- [10] E. Derevtsov and I. Svetov, *Tomography of tensor fields in the plane*, Eurasian J. Math. Comput. Appl., **3**(2) (2015), 24–68.
- [11] E. Derevtsov, Y. Volkov and T. Schuster, *Generalized attenuated ray transforms and their integral angular moments*, Appl. Math. and Comput., **409** (2021), 125494.
- [12] A. Denisiuk, *Iterative inversion of the tensor momentum x -ray transform*, Inverse Problems **39** (10), (2023), 105002.
- [13] N. Desai and W. Lionheart, *An explicit reconstruction algorithm for the transverse ray transform of a second rank tensor field from three axis data*, Inverse Problems, **32**(11), (2016), 115009.
- [14] D. V. Finch, *The attenuated x -ray transform: recent developments*, in Inside out: inverse problems and applications, Math. Sci. Res. Inst. Publ., **47**, Cambridge Univ. Press, Cambridge, 2003, 47–66.
- [15] H. Fujiwara, K. Sadiq and A. Tamasan, *A Fourier approach to the inverse source problem in an absorbing and anisotropic scattering medium*, Inverse Problems **36**(1):015005 (2019).
- [16] H. Fujiwara, K. Sadiq and A. Tamasan, *Numerical reconstruction of radiative sources in an absorbing and non-diffusing scattering medium in two dimensions*, SIAM J. Imaging Sci., **13**(1) (2020), 535–555.
- [17] S. Haider, A. Hrbek and Y. Xu, *Magneto-acousto-electrical tomography: a potential method for imaging current density and electrical impedance* Physiol. Meas. **29** (2008) 41–50.
- [18] J. Hendriks, A. Gregg, C. Wensrich, A. Tremsin, T. Shinohara, M. Meylan, E. Kisi, V. Luzin, O. Kirsten, *Bragg-edge elastic strain tomography for in situ systems from energy-resolved neutron transmission imaging*, Physical Review Materials **1** (5) (2017) 053802.
- [19] S. Holman and P. Stefanov, *The weighted Doppler transform*, Inverse Probl. Imaging, **4** (2010), 111–130.
- [20] S. G. Kazantsev and A. A. Bukhgeim, *Inversion of the scalar and vector attenuated X -ray transforms in a unit disc*, J. Inverse Ill-Posed Probl., **15** (2007), 735–765.
- [21] V. P. Krishnan, R. Manna, S. K. Sahoo, and V. A. Sharafutdinov, *Momentum ray transforms*, Inverse Problems Imaging **3** (13) (2019), 679–701.
- [22] V. P. Krishnan, R. Mishra and F. Monard *On solenoidal-injective and injective ray transforms of tensor fields on surfaces*, J. Inverse Ill-Posed Problems **27** (4) (2019), 527–538.
- [23] L. Kunyansky, E. McDugald, and B. Shearer, *Weighted Radon transforms of vector fields, with applications to magnetoacoustoelectric tomography*, Inverse Problems **39** (6) (2023), 065014.
- [24] A. Louis, *Inversion formulae for ray transforms in vector and tensor tomography*, Inverse Problems **38**:065008 (2022).
- [25] R. K. Mishra, *Full reconstruction of a vector field from restricted Doppler and first integral moment transforms in \mathbb{R}^n* , J. Inverse Ill-Posed Problems **28** (2019), 173–184.
- [26] R. K. Mishra and S. K. Sahoo, *Injectivity and range description of integral moment transforms over m -tensor fields in \mathbb{R}^n* , SIAM J. Math. Anal., **53** (1), (2021), 253–278.
- [27] F. Natterer, *The mathematics of computerized tomography*, Wiley, New York, 1986.
- [28] S. J. Norton, *Tomographic reconstruction of 2-D vector fields: application to flow imaging*, Geophysical Journal **97** (1) (1989), 161–168.
- [29] V. Palamodov, *Reconstruction of a differential form from doppler transform*, SIAM Journal on Mathematical Analysis, **41**(4) (2009), 1713–1720.

- [30] G. P. Paternain, M. Salo, and G. Uhlmann, *Tensor Tomography: Progress and Challenges*, Chin. Ann. Math. Ser. B., **35(3)** (2014), 399–428.
- [31] L. Pestov and G. Uhlmann, *On characterization of the range and inversion formulas for the geodesic X-ray transform*, Int. Math. Res. Not., **80** (2004), 4331–4347.
- [32] K. Sadiq and A. Tamasan, *On the range of the attenuated Radon transform in strictly convex sets*, Trans. Amer. Math. Soc., **367(8)** (2015), 5375–5398.
- [33] K. Sadiq and A. Tamasan, *On the range characterization of the two dimensional attenuated Doppler transform*, SIAM J. Math. Anal., **47(3)** (2015), 2001–2021.
- [34] K. Sadiq, A. Tamasan, *On the range of the X-ray transform of symmetric tensors compactly supported in the plane*, Inverse Probl. Imaging **17(3)** (2023), 660–685.
- [35] K. Sadiq, O. Scherzer, and A. Tamasan, *On the X-ray transform of planar symmetric 2-tensors*, J. Math. Anal. Appl., **442(1)** (2016), 31–49.
- [36] T. Schuster, *20 years of imaging in vector field tomography: a review*. In Y. Censor, M. Jiang, A.K. Louis (Eds.), *Mathematical Methods in Biomedical Imaging and Intensity-Modulated Radiation Therapy (IMRT)*, in: Publications of the Scuola Normale Superiore, CRM **7** (2008) 389–424.
- [37] V. A. Sharafutdinov, *Integral geometry of tensor fields*, VSP, Utrecht, 1994.
- [38] V. A. Sharafutdinov, *The Reshetnyak formula and Natterer stability estimates in tensor tomography*, Inverse Problems, **33(2)** (2017), 025002.
- [39] G. Sparr, K. Stråhlén, K. Lindström, and H. W. Persson, *Doppler tomography for vector fields*, Inverse Problems, **11** (1995), 1051–1061.
- [40] P. Stefanov, and G. Uhlmann, *Rigidity for metrics with same lengths of geodesics*, Math. Res. Lett., **5**, (1998) 83–96.
- [41] P. Stefanov, G. Uhlmann, A. Vasy, and H. Zhou, *Travel time tomograph*, Acta Math. Sin. (Engl. Ser.), **35(6)** (2019), 1085–1114.
- [42] A. Tamasan, *Tomographic reconstruction of vector fields in variable background media*, Inverse Problems **23** (2007), 2197–2205.
- [43] I. N. Vekua, *Generalized Analytic Functions*, Pergamon Press Ltd. 1962.

GRADUATE SCHOOL OF INFORMATICS, KYOTO UNIVERSITY, YOSHIDA HONMACHI, SAKYO-KU, KYOTO 606-8501, JAPAN

Email address: fujiwara@acs.i.kyoto-u.ac.jp

FACULTY OF MATHEMATICS, COMPUTATIONAL SCIENCE CENTER, UNIVERSITY OF VIENNA, OSKAR-MORGENSTERN-PLATZ 1, 1090 VIENNA, AUSTRIA

Email address: david.omogbhe@univie.ac.at

JOHANN RADON INSTITUTE FOR COMPUTATIONAL AND APPLIED MATHEMATICS (RICAM), ALTENBERGER-STRASSE 69, 4040 LINZ, AUSTRIA

Email address: kamran.sadiq@ricam.oeaw.ac.at

DEPARTMENT OF MATHEMATICS, UNIVERSITY OF CENTRAL FLORIDA, ORLANDO, 32816 FLORIDA, USA

Email address: tamasan@math.ucf.edu